Suppression of heating by multicolor driving protocols in Floquet-engineered strongly correlated systems

Yuta Murakami [1,*] Michael Schüler, [2,3] Ryotaro Arita [1,4] and Philipp Werner [3]

[1]*Center for Emergent Matter Science, RIKEN, Wako, Saitama 351-0198, Japan*
[2]*Laboratory for Theoretical and Computational Physics, Paul Scherrer Institut, 5232 Villigen PSI, Switzerland*
[3]*Department of Physics, University of Fribourg, 1700 Fribourg, Switzerland*
[4]*Research Center for Advanced Science and Technology, University of Tokyo, Komaba, Tokyo 153-8904, Japan*

Heating effects in Floquet-engineered systems are detrimental to the control of physical properties. In this paper, we show that the heating of periodically driven strongly correlated systems can be suppressed by multicolor driving, i.e., by applying auxiliary excitations which interfere with the absorption processes from the main drive. We focus on the Mott insulating single-band Hubbard model and study the effects of multicolor driving with nonequilibrium dynamical mean-field theory. The main excitation is a periodic electric field with frequency Ω smaller than the Mott gap, while for the auxiliary excitations, we consider additional electric fields and/or hopping modulations with a higher harmonic of Ω. To suppress the three-photon absorption of the main excitation, which is a parity-odd process, we consider auxiliary electric-field excitations and a combination of electric-field excitations and hopping modulations. On the other hand, to suppress the two-photon absorption, which is a parity-even process, we consider hopping modulations. The conditions for an efficient suppression of heating are well captured by the Floquet effective Hamiltonian derived with the high-frequency expansion in a rotating frame. As an application, we focus on the exchange couplings of the spins (pseudospins) in the repulsive (attractive) model and demonstrate that the suppression of heating allows us to realize and clearly observe a significant Floquet-induced change of the low energy physics.

I. INTRODUCTION

Floquet engineering, where a system is exposed to strong periodic excitations, provides a promising pathway to control the physical properties of a system [1–3]. Theoretical predictions of Floquet engineering effects range from the realization of Floquet topological insulators in weakly correlated systems [4–7], Floquet topological superconductivity [8–10], control of band structures [11,12] and electron-phonon couplings [13–15], to control of magnetisms in strongly correlated systems [16–19]. Experimentally, driving-induced band renormalizations [20–22], the creation of topological band structures [23,24], and the control of exchange couplings in strongly correlated systems [25] have been demonstrated in cold atom systems. In real materials, the realization of a Floquet-induced anomalous Hall effect has also been experimentally reported in graphene [26], although the interpretation of the result is not yet fully settled [27]. More recently, light-induced anomalous Hall effects are also reported in three-dimensional Dirac systems like Co_3SnS_2 [28] and bismuth [29]. In addition, giant modifications of the nonlinear response by Floquet engineering have been reported in a correlated material [30]. Still, compared with the broad range of theoretical predictions, experimental realizations of Floquet engineering are still limited.

One of the major difficulties in implementing Floquet engineering approaches in practice is the heating of the system, which may hinder the clear emergence of topological properties and the change in low-energy physics. Heating can occur at different levels. For example, in real systems, there always exist bands above the targeted low-lying bands which most theoretical studies focus on. Strong excitations can excite particles from the target bands to the high-energy bands, which may prevent the realization of the intended Floquet engineering effect. Another possibility is excitations within the target bands. Due to the nonthermal or hot distribution caused by such excitations, the control of topological properties and low-energy physics becomes difficult to observe [7]. A promising way to avoid heating is to use multicolor driving protocols [31,32], which also provide further controllability of the system [33–36]. Recently, such a protocol has been implemented in a cold atom system to suppress the excitation of particles to higher energy bands [31], while optimal control theory has been used to engineer the band filling in a free system under periodic driving [32]. However, to what extent multicolor driving protocols are beneficial for the Floquet engineering of strongly correlated systems remains to be understood. Rich low-energy physics and phases resulting from the competition or cooperation between various degrees of freedoms are characteristic of strongly correlated systems. If heating can be suppressed, such low-energy physics and phases can be efficiently controlled by Floquet engineering.

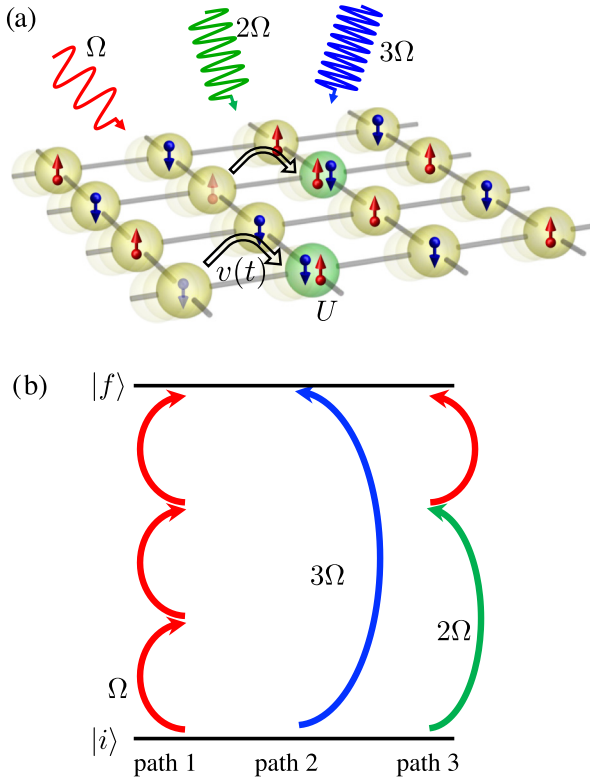---

*yuta.murakami@riken.jp

035151-1

FIG. 1. (a) Schematic picture of the Hubbard model excited with multicolor driving protocols. The red wavy line indicates the main excitation with frequency Ω, while the green and blue wavy lines indicate auxiliary excitations with higher harmonics of Ω. (b) Illustration of the basic idea behind the cancellation of absorption processes using multicolor excitations. The red arrows indicate the three-photon excitation from the main drive with frequency Ω. The blue and green arrows indicate auxiliary 3Ω and 2Ω excitations, respectively. $|i\rangle$ represents the initial state, while $|f\rangle$ represents the final state.

In this paper, we address this question by analyzing the half-filled single-band Hubbard model, a standard model for strongly correlated systems, with the nonequilibrium dynamical mean-field theory (DMFT) [37,38]. Specifically, we focus on Mott insulators and consider an electric field excitation with frequency Ω as the main excitation, which is chosen to be a subgap driving. Additional electric fields and hopping modulations with higher harmonics of Ω are used as auxiliary excitations, see Fig. 1(a). We discuss and demonstrate how the three-photon and two-photon absorption can be reduced by suppressing the doublon-holon (d-h) creation/annihilation terms in the Floquet effective Hamiltonian. The resulting suppression of heating allows us to directly observe the change of the exchange couplings due to the virtual excitations induced by the periodic excitations.

This paper is organized as follows. In Sec. II, we introduce the Hubbard model and derive the corresponding Floquet Hamiltonian using the high-frequency expansion in a rotating frame. Then we discuss how the Floquet Hamiltonian allows us to determine conditions for the efficient suppression of heating. In Sec. III, we study the real-time dynamics of the system with a repulsive or attractive interaction using

nonequilibrium DMFT and demonstrate how the suppression of heating in the multicolor protocols works. Conclusions are given in Sec. IV.

II. FORMALISM

A. Model

In this paper, we consider the single-band Hubbard model

$$\hat{H}(t) = - \sum_{\langle i,j \rangle, \sigma} v_{ij}(t) \hat{c}_{i\sigma}^\dagger \hat{c}_{j\sigma} + U \sum_j \hat{n}_{j\uparrow} \hat{n}_{j\downarrow}, \qquad (1)$$

where $\hat{c}_{i\sigma}^\dagger$ is the creation operator for a fermionic particle with spin σ at site i, $\langle ij \rangle$ indicates a pair of neighboring sites, and $\hat{n}_{i\sigma} = \hat{c}_{i\sigma}^\dagger \hat{c}_{i\sigma}$. Here, U is the on-site interaction, and $v_{ij}(t)$ is the time-dependent hopping parameter. We consider two basic excitation protocols. The first one is an electric field excitation, which enters the calculation via the Peierls substitution [38] $v_{ij}(t) = v_0 \exp[i\mathbf{A}(t) \cdot \mathbf{r}_{ij}]$. Here, v_0 is the equilibrium hopping parameter, $\mathbf{A}(t)$ is the vector potential, and $\mathbf{r}_{ij}$ is the vector from the j site to the i site. The charge of the particle and the bond length are set to unity. The electric field is related to the vector potential by $\mathbf{E}(t) = -\partial_t \mathbf{A}(t)$. The second protocol is the hopping modulation, which corresponds to $v_{ij}(t) = v_0 + \delta v(t)$. Both of these protocols have been implemented in cold-atom systems [1,22,31]. In real materials, electric field excitations can be implemented easily, while hopping modulations may be achieved via the excitation of coherent phonons [39,40].

In this paper, we consider systems on bipartite lattices, i.e., the Bethe lattice or hypercubic lattices, at half-filling. We consider models with strong repulsive or strong attractive interactions to discuss the effects of multicolor driving for different types of orders (low-energy physics). When U is repulsive ($U > 0$), the system favors singly occupied sites (singlons) in equilibrium and exhibits an antiferromagnetic (AFM) phase at low enough temperatures. The absorption of energy of $O(U)$ creates doubly occupied sites (doublons) and empty sites (holons), which can destroy the low-energy spin order [41,42]. When U is attractive ($U < 0$), the system favors doublons and holons in equilibrium and shows s-wave superconductivity, charge order, or a coexistence of both at low enough temperatures. This physics originates from the SU(2) symmetry which corresponds to the spin SU(2) symmetry of the repulsive Hubbard model via the Shiba transformation. The absorption of an energy of $O(|U|)$ in the attractive model creates singlons.

For simplicity, we apply the electric field along a high-symmetry direction. In the case of the hypercubic lattices, this is the body-diagonal direction. More specifically, if we denote the unit vector along the a axis by $\mathbf{e}_a$, we consider a field along $\mathbf{e}_{\mathrm{BD}} \equiv \sum_a \mathbf{e}_a$. As we will mention below, the Bethe lattice can also mimic this situation.

In this paper, we consider four types of excitation protocols, see Table I. The most basic one, which we call type 0, is the conventional single-color electric field excitation. This corresponds to $v_{ij}(t) = v_0 \exp[i\mathbf{A}(t) \cdot \mathbf{r}_{ij}]$, with

$$\mathbf{A}(t) = \mathbf{e}_{\mathrm{BD}} A_0 \sin(\Omega t). \qquad (2)$$

TABLE I. Summary of excitation protocols.

Name	Involved processes	Relevant Eq.
Type 0	Single-color electric field	Eq. (2)
Type 1	Two-color electric field	Eq. (3)
Type 2	Single-color electric field	Eq. (4)
	+ single-color hopping modulation	
Type 3	Two-color electric field	Eq. (5)
	+ single-color hopping modulation	

This electric field excitation with frequency Ω, which is chosen to be smaller than the Mott gap, represents the primary excitation, and we try to suppress the associated heating (absorption) processes with additional weaker excitations. In the case of type-1 excitations, we consider an additional electric field excitation with frequency $n_1\Omega$, where n_1 is an integer. Specifically, we set $v_{ij}(t) = v_0 \exp[i\mathbf{A}(t) \cdot \mathbf{r}_{ij}]$, with

$$\mathbf{A}(t) = \mathbf{e}_{\mathrm{BD}}[A_0 \sin(\Omega t) + A_1 \sin(n_1\Omega t + \phi_1)]. \quad (3)$$

Here, ϕ_1 is the phase shift of the second field relative to the main drive. In type-2 excitations, we consider an additional hopping modulation with frequency $n_2\Omega$, i.e., we set $v_{ij}(t) = v_0[1 + \delta v(t)] \exp[i\mathbf{A}(t) \cdot \mathbf{r}_{ij}]$ with

$$\mathbf{A}(t) = \mathbf{e}_{\mathrm{BD}}A_0 \sin(\Omega t),$$
$$\delta v(t) = \delta_v \cos(n_2\Omega t + \phi_2). \quad (4)$$

Here, ϕ_2 is the phase shift of the hopping modulation. In type-3 excitations, we use both an additional electric field excitation with frequency $n_1\Omega$ and a hopping modulation with frequency $n_2\Omega$. This corresponds to $v_{ij}(t) = v_0[1 + \delta v(t)] \exp[i\mathbf{A}(t) \cdot \mathbf{r}_{ij}]$, with

$$\mathbf{A}(t) = \mathbf{e}_{\mathrm{BD}}[A_0 \sin(\Omega t) + A_1 \sin(n_1\Omega t + \phi_1)],$$
$$\delta v(t) = \delta_v \cos(n_2\Omega t + \phi_2). \quad (5)$$

B. Floquet Hamiltonians in the rotating frame and suppression of absorption

The idea underlying the suppression of heating with multicolor excitations is based on cancellations between different excitation processes. Let us consider an excitation process from $|i\rangle$ to $|f\rangle$ using m photons from the electric field excitation of frequency Ω, see Fig. 1(b). With additional fields with higher harmonics of Ω, it is possible to create other excitations from $|i\rangle$ to $|f\rangle$, which can interfere with the main excitation process. In the perturbative regime with respect to the field strength, the amplitude of the m-photon process of the main field is $O(A_0^m)$. The amplitude of the interfering processes produced by the additional fields should be of the same order. For example, the strength of an additional field A' with frequency $m\Omega$, whose first-order processes interfere with the m-photon processes of the Ω-frequency field, should be $A' \simeq O(A_0^m)$. Hence, A' can be much weaker than the main field. For this reason, we refer to the additional fields as auxiliary fields. Although such cancellations can be discussed in detail within the framework of time-dependent perturbation

theory, an alternative and simpler option is to analyze the Floquet Hamiltonian, as will be done below.

In the following, we consider subgap excitations where $U = l_0\Omega + \Delta U$ (l_0 is an integer) and assume that $|U|, \Omega \gg |v_0|, |\Delta U|$. Following Ref. [43], we can derive the effective Floquet Hamiltonian, applying the high-frequency expansion in a rotating frame. This procedure allows us to deal with the effects of U and Ω on equal footing, and the resultant effective Hamiltonian naturally includes the absorption processes and the exchange couplings from virtual excitations due to periodic excitations, as seen below. First, introducing $U_0 \equiv l_0\Omega$, we switch to the rotating frame defined by a unitary transformation $\hat{\mathcal{U}}(t) = \exp(-iU_0 t \sum_j \hat{n}_{j\uparrow}\hat{n}_{j\downarrow})$ by calculating $|\psi^{\mathrm{rot}}(t)\rangle = \hat{\mathcal{U}}^\dagger(t)|\psi(t)\rangle$. The resultant Hamiltonian in the rotating frame ($\hat{H}^{\mathrm{rot}}(t) = \hat{\mathcal{U}}^\dagger(t)\hat{H}(t)\hat{\mathcal{U}}(t) + i(\partial_t\hat{\mathcal{U}}^\dagger(t))\hat{\mathcal{U}}(t)$) is

$$\hat{H}^{\mathrm{rot}}(t) = - \sum_{\langle i,j\rangle,\sigma} \{v_{ij}(t)\hat{g}_{ij\sigma} + [v_{ij}(t)\exp(iU_0 t)\hat{h}_{ij\sigma}^\dagger + \mathrm{H.c.}]\}$$
$$+ \Delta U \sum_j \hat{n}_{j\uparrow}\hat{n}_{j\downarrow}. \quad (6)$$

Here, we introduced $\hat{g}_{ij\sigma} = (1 - \hat{n}_{i\bar{\sigma}})\hat{c}_{i\sigma}^\dagger \hat{c}_{j\sigma}(1 - \hat{n}_{j\bar{\sigma}}) + \hat{n}_{i\bar{\sigma}}\hat{c}_{i\sigma}^\dagger \hat{c}_{j\sigma}\hat{n}_{j\bar{\sigma}}$ and $\hat{h}_{ij\sigma}^\dagger = \hat{n}_{i\bar{\sigma}}\hat{c}_{i\sigma}^\dagger \hat{c}_{j\sigma}(1 - \hat{n}_{j\bar{\sigma}})$. The former operator does not change the number of doublons and holons, and the latter is the generator of them. Assuming $\Omega \gg |v_0|, |\Delta U|$, we apply the high-frequency expansion to the Hamiltonian in Eq. (6) and obtain the effective Floquet Hamiltonian

$$\hat{H}_{\mathrm{eff}} = \hat{H}_0^{\mathrm{rot}} + \sum_{l>0} \frac{[\hat{H}_l^{\mathrm{rot}}, \hat{H}_{-l}^{\mathrm{rot}}]}{l\Omega} + O\left(\frac{1}{\Omega^2}\right). \quad (7)$$

Here, $\hat{H}^{\mathrm{rot}}(t) = \sum_l \hat{H}_l^{\mathrm{rot}}e^{il\Omega t}$. We note that this effective Hamiltonian can describe the stroboscopic time evolution of the system [44]. To express $\hat{H}_l^{\mathrm{rot}}$, we introduce the Fourier components $\mathcal{A}^{(l)}$ defined by $v_{ij}(t) = v_0 \sum_l \mathcal{A}_{ij}^{(l)} e^{il\Omega t}$ and set $\mathcal{B}_{ij}^{(l)} \equiv \mathcal{A}_{ij}^{(l-l_0)}$, where $v_{ij}(t)\exp(iU_0 t) = v_0 \sum_l \mathcal{A}_{ij}^{(l)} \exp[i(l + l_0)\Omega t] = v_0 \sum_l \mathcal{B}_{ij}^{(l)} e^{il\Omega t}$ is full-filled.

The lowest-order Hamiltonian is

$$\hat{H}_0^{\mathrm{rot}} = -v_0 \sum_{\langle ij\rangle\sigma} \{\mathcal{A}_{ij}^{(0)}\hat{g}_{ij\sigma} + [\mathcal{B}_{ij}^{(0)}\hat{h}_{ij\sigma}^\dagger + \mathrm{H.c.}]\}$$
$$+ \Delta U \sum_j \hat{n}_{j\uparrow}\hat{n}_{j\downarrow}. \quad (8)$$

Remember that $\mathcal{B}_{ij}^{(0)} = \mathcal{A}_{ij}^{(-l_0)}$ is a Fourier component of the time-dependent hopping amplitude of the original Hamiltonian in Eq. (1) and corresponds to the amplitude for the instantaneous absorption of the energy $l_0\Omega$. For $l \neq 0$, we have

$$\hat{H}_l^{\mathrm{rot}} = -v_0 \sum_{\langle ij\rangle\sigma} \{\mathcal{A}_{ij}^{(l)}\hat{g}_{ij\sigma} + [\mathcal{B}_{ij}^{(l)}\hat{h}_{ij\sigma}^\dagger + \mathcal{B}_{ij}^{(-l)*}\hat{h}_{ij\sigma}]\}. \quad (9)$$

Therefore, as far as the leading-order Hamiltonian is concerned, if $\mathcal{B}^{(0)} = 0$, there is no creation of doublons and holons.
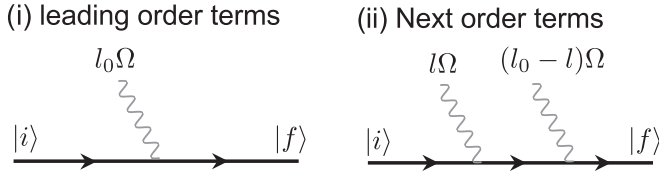
FIG. 2. Schematic picture of excitation processes corresponding to the doublon-holon creation/annihilation terms in the Floquet Hamiltonian.

The second-order term $O(\frac{v_0^2}{\Omega})$ can be expressed as $\hat{H}_{\text{eff}}^{(2)} = \hat{H}_{\text{eff},1}^{(2)} + \hat{H}_{\text{eff},2}^{(2)} + \hat{H}_{\text{eff},3}^{(2)}$, with

$$\hat{H}_{\text{eff},1}^{(2)} = \sum_{l>0} \frac{v_0^2}{l\Omega} \left[\sum_{\langle ij \rangle \sigma} \mathcal{A}_{ij}^{(l)} \hat{g}_{ij\sigma}, \sum_{\langle i'j' \rangle \sigma'} \mathcal{A}_{i'j'}^{(-l)} \hat{g}_{i'j'\sigma'} \right], \quad (10a)$$

$$\hat{H}_{\text{eff},2}^{(2)} = \sum_{l\neq0} \frac{v_0^2}{l\Omega} \left[\sum_{\langle ij \rangle \sigma} \mathcal{A}_{ij}^{(l)} \hat{g}_{ij\sigma}, \sum_{\langle i'j' \rangle \sigma'} \left[\mathcal{B}_{i'j'}^{(-l)} \hat{h}_{i'j'\sigma'}^{\dagger} + \mathcal{B}_{i'j'}^{(l)*} \hat{h}_{i'j'\sigma'} \right] \right], \quad (10b)$$

$$\hat{H}_{\text{eff},3}^{(2)} = \sum_{l\neq0} \frac{v_0^2}{l\Omega} \left[\sum_{\langle ij \rangle \sigma} \mathcal{B}_{ij}^{(l)} \hat{h}_{ij\sigma}^{\dagger}, \sum_{\langle i'j' \rangle \sigma'} \mathcal{B}_{i'j'}^{(l)*} \hat{h}_{i'j'\sigma'} \right]. \quad (10c)$$

Here, $\hat{H}_{\text{eff},2}^{(2)}$ describes the creation and annihilation processes of doublons and holons and is relevant for absorption (heating) processes [45]. The remaining terms do not change the number of doublons and holons and govern the low-energy physics, which we discuss in detail in the next section. The full expressions for $\hat{H}_{\text{eff},2}^{(2)}$ and $\hat{H}_{\text{eff},3}^{(2)}$ are given in Appendix B. Note that the expressions in Eqs. (8)–(10) are generic and not limited to electric field excitations along $\mathbf{e}_{\text{BD}}$.

Now let us discuss the meaning of the d-h creation/annihilation terms in the effective Floquet Hamiltonian, i.e., Eqs. (8) and (10). Firstly, these terms only describe the $l_0\Omega$ absorption processes, while possible $l(\neq l_0)\Omega$ absorption processes are not included. To express the latter processes, one needs to consider the effective Hamiltonian in the rotating frame of $e^{il\Omega}$. Secondly, $\mathcal{A}^{(l)}$ corresponds to simultaneous $l\Omega$ excitations, as can be seen from its definition. Therefore, the leading order d-h creation/annihilation processes in Eq. (8) correspond to the simultaneous absorption of $l_0\Omega$, while the next-leading-order terms in Eq. (10b) correspond to the absorption of $l\Omega$ and $(l_0 - l)\Omega$ at different times, see Fig. 2. Thirdly, $\mathcal{A}^{(l)}$ already includes the contribution from different excitation processes since $v(t)$ depends in a nonlinear manner on $A(t)$, see Eqs. (19) and (21) below, for example. This allows us to suppress some $\mathcal{A}^{(l)}$ by tuning the parameters of the auxiliary fields. We also emphasize that the effective Hamiltonian can be applied in the nonperturbative regime with respect to the field strength.

We note that the effects of the interference between the main field and the auxiliary fields can appear in the effective Floquet Hamiltonian at different levels. On the one hand, it can affect the value of $\mathcal{A}^{(l)}$ and thus can modify the coefficients of the d-h creation/annihilation terms. On the other hand, interferences can also occur between different

processes expressed by different terms in the effective Hamiltonian. In the following, to find the conditions for the efficient suppression of heating, we follow the strategy to suppress the d-h creation/annihilation terms in the Floquet Hamiltonian order by order. This strategy should work in the high-frequency limit ($\Omega \gg |v_0|, |\Delta U|$), but for moderate values of Ω, it is not *a priori* clear how well this strategy works. For example, a condition which eliminates the leading-order terms may enhance contributions from the next order. Furthermore, this strategy does not consider the potential interferences between the different processes described by the terms representing different orders. It aims to suppress the $l_0\Omega$ absorption processes only, which is reasonable when such processes are the dominant ones. We also note that the auxiliary field may enhance or suppress $l\Omega$ ($l \neq l_0$) absorptions. Despite these potential difficulties, we will show that the Floquet Hamiltonian serves as a useful guide to determine conditions for the efficient suppression of heating in the present system.

For an electric field excitation along $\mathbf{e}_{\text{BD}}$, $\mathcal{A}_{ij}^{(l)}$ can take only two possible values for a given l, namely, $\mathcal{A}_{\mathbf{e}_a}^{(l)}$ or $\mathcal{A}_{-\mathbf{e}_a}^{(l)}$. In the following, we denote them by $\mathcal{A}_{\mathbf{e}}^{(l)}$ and $\mathcal{A}_{-\mathbf{e}}^{(l)}$, respectively. The same notation is used for $\mathcal{B}_{ij}^{(l)}$. With this, the coefficients appearing in $\hat{H}_{\text{eff},2}^{(2)}$ can be classified into the following four cases and their complex conjugates:

$$I_1^{(\text{dh})} = \sum_{l\neq0} \frac{1}{l} \mathcal{A}_{\mathbf{e}}^{(l)} \mathcal{B}_{\mathbf{e}}^{(-l)}, \quad I_1^{(\text{dh})'} = \sum_{l\neq0} \frac{1}{l} \mathcal{A}_{-\mathbf{e}}^{(l)} \mathcal{B}_{-\mathbf{e}}^{(-l)},$$

$$I_2^{(\text{dh})} = \sum_{l\neq0} \frac{1}{l} \mathcal{A}_{\mathbf{e}}^{(l)} \mathcal{B}_{-\mathbf{e}}^{(-l)}, \quad I_2^{(\text{dh})'} = \sum_{l\neq0} \frac{1}{l} \mathcal{A}_{-\mathbf{e}}^{(l)} \mathcal{B}_{\mathbf{e}}^{(-l)}. \quad (11)$$

The relevant question then becomes how to suppress $\mathcal{B}^{(0)}$ and these coefficients.

C. Floquet-engineered exchange couplings

From $\hat{H}_{\text{eff},1}^{(2)} + \hat{H}_{\text{eff},3}^{(2)}$, one can obtain the effective model for the low-energy physics. Here, $\hat{H}_{\text{eff},3}^{(2)}$ includes the exchange terms for spins and pseudospins (doublons and holons), which control the low-energy physics if $O(|U|)$ absorption from the equilibrium state is absent. These terms yield Heisenberg-type Hamiltonians both in the repulsive and attractive cases. To simplify the expression of the Hamiltonian, we focus on the case where $\mathcal{A}_{\mathbf{e}}^{(l)} = \mathcal{A}_{-\mathbf{e}}^{(l)}(-)^l$ and these coefficients are real. This condition is fulfilled for the four excitation protocols mentioned above if $\phi_1 = \phi_2 = 0$, $n_1 = \text{odd}$, and $n_2 = \text{even}$. We mainly focus on this situation in the following. We note that this condition implies $I_1^{(\text{dh})'} \propto I_1^{(\text{dh})}$, $I_2^{(\text{dh})'} \propto I_2^{(\text{dh})}$, and $\hat{H}_{\text{eff},1}^{(2)} = 0$.

When U is repulsive, the low-energy physics is described by the spin degrees of freedom. From $\hat{H}_{\text{eff},3}^{(2)}$ (see Appendix B), the low-energy Hamiltonian consisting of the spin exchange terms can be expressed as

$$\hat{H}_{\text{spin}} = J_s^{(\text{HE})} \sum_{\langle ij \rangle} \hat{\mathbf{s}}_i \cdot \hat{\mathbf{s}}_j. \quad (12)$$

Here, (ij) indicates a pair of neighboring sites, $(ij) = (ji)$ and

$$J_s^{(\text{HE})} = \sum_{l \neq 0} \frac{4v_0^2}{l\Omega} |\mathcal{B}_\mathbf{e}^{(l)}|^2. \quad (13)$$

The spin operators are $\hat{\mathbf{s}} = \frac{1}{2} \sum_{\alpha,\beta=\uparrow,\downarrow} \hat{c}_\alpha^\dagger \boldsymbol{\sigma}_{\alpha\beta} \hat{c}_\beta$, with $\boldsymbol{\sigma}$ denoting the Pauli matrices. HE stands for high-frequency expansion. In equilibrium, $J_s^{(\text{HE})} = \frac{4v_0^2}{U_0} > 0$ since $\mathcal{B}^{(l_0)} = 1$.

In a system with strong attractive interactions, the equilibrium state favors doublons or holons. To express the low-energy Hamiltonian, we introduce the pseudospins defined in the space of these local states as $\hat{\eta}_i^+ = (-)^i \hat{c}_{i\downarrow}^\dagger \hat{c}_{i\uparrow}^\dagger$, $\hat{\eta}_i^- = (-)^i \hat{c}_{i\uparrow} \hat{c}_{i\downarrow}$ and $\hat{\eta}_i^z = \frac{1}{2}(\hat{n}_i - 1)$. Here, $(-)^i = 1$ for the A sublattice, and $(-)^i = -1$ for the B sublattice. The low-energy Hamiltonian can be expressed as

$$\hat{H}_{\text{dh}} = J_{\eta,XY}^{(\text{HE})} \sum_{(ij)} \left(\hat{\eta}_i^x \hat{\eta}_j^x + \hat{\eta}_i^y \hat{\eta}_j^y \right) + J_{\eta,Z}^{(\text{HE})} \sum_{(ij)} \hat{\eta}_i^z \hat{\eta}_j^z, \quad (14)$$

where

$$J_{\eta,XY}^{(\text{HE})} = -\sum_{l \neq 0} \frac{4v_0^2}{l\Omega} \mathcal{B}_\mathbf{e}^{(l)} \mathcal{B}_{-\mathbf{e}}^{(l)}, \quad (15a)$$

$$J_{\eta,Z}^{(\text{HE})} = -\sum_{l \neq 0} \frac{4v_0^2}{l\Omega} |\mathcal{B}_\mathbf{e}^{(l)}|^2. \quad (15b)$$

In equilibrium, $J_{\eta,XY}^{(\text{HE})} = J_{\eta,Z}^{(\text{HE})} = -\frac{4v_0^2}{U_0} > 0$, which can be connected to the spin SU(2) symmetry in the repulsive Hubbard model via the Shiba transformation. However, under the electric field, $J_{\eta,XY}^{(\text{HE})} \neq J_{\eta,Z}^{(\text{HE})}$ in general [46]. We again note that these expressions are justified when $\Omega, |U| \gg v_0, |\Delta U|$. For the following analysis, we introduce $I_1^{(\text{ex})} = \sum_{l \neq 0} \frac{1}{l} |\mathcal{B}_\mathbf{e}^{(l)}|^2$ and $I_2^{(\text{ex})} = \sum_{l \neq 0} \frac{1}{l} \mathcal{B}_\mathbf{e}^{(l)} \mathcal{B}_{-\mathbf{e}}^{(l)}$.

On the other hand, for $\Omega, |U|, |\Delta U| \gg |v_0|$, we obtain slightly different expressions for the exchange couplings. In this case, we consider the Floquet space (extended Hilbert space with photodressed states) and apply degenerate perturbation theory [16,46]. For example, for $U > 0$, starting from states with only singly occupied sites, we consider virtual excitations to states with a d-h pair dressed with l photons, where the transition amplitude is proportional to $\mathcal{A}^{(-l)}$. As a result, we have $\hat{H}_{\text{spin}} = J_s^{(P)} \sum_{(ij)} \hat{\mathbf{s}}_i \cdot \hat{\mathbf{s}}_j$, with

$$J_s^{(P)} = \sum_l \frac{4v_0^2}{U - l\Omega} |\mathcal{A}_\mathbf{e}^{(-l)}|^2. \quad (16)$$

Similarly, for $U < 0$, we have $\hat{H}_{\text{dh}} = J_{\eta,XY}^{(P)} \sum_{(ij)} (\hat{\eta}_i^x \hat{\eta}_j^x + \hat{\eta}_i^y \hat{\eta}_j^y) + J_{\eta,Z}^{(P)} \sum_{(ij)} \hat{\eta}_i^z \hat{\eta}_j^z$, with

$$J_{\eta,XY}^{(P)} = -\sum_l \frac{4v_0^2}{U - l\Omega} \mathcal{A}_\mathbf{e}^{(-l)} \mathcal{A}_{-\mathbf{e}}^{(-l)}, \quad (17a)$$

$$J_{\eta,Z}^{(P)} = -\sum_l \frac{4v_0^2}{U - l\Omega} |\mathcal{A}_\mathbf{e}^{(-l)}|^2. \quad (17b)$$

Note that these expressions break down at the resonance condition $U = l_0\Omega$, but without the diverging term $l = l_0$, $J^{(P)}$ becomes equal to $J^{(\text{HE})}$. The same expression can be obtained by introducing Ω_0 such that $\Omega = k_0\Omega_0$ and $U = l_0\Omega_0$, where

k_0 and l_0 have no common integer factor >1. More specifically, we consider the rotating frame of e^{iUt} and apply the high-frequency expansion in terms of Ω_0 [43]. For practical values of $|U|$ and off-resonant conditions, it is not *a priori* clear whether Eqs. (13) and (15) or Eqs. (16) and (17) provide a better description of the low-energy properties.

D. Assessment of the different protocols

In this section, we evaluate $\mathcal{A}_\mathbf{e}^{(l)}(= \mathcal{A}_{-\mathbf{e}}^{(-l)*})$ for each excitation protocol and determine the condition for the suppression of the d-h creation terms in the Floquet Hamiltonian.

1. Type-1 excitation

In the type-1 protocol, in addition to the basic excitation by an electric field with frequency Ω, we consider an electric field excitation of the form given in Eq. (3). Then we have

$$\mathcal{A}_\mathbf{e}^{(l)} = \frac{1}{2\pi} \int_0^{2\pi} \exp\{i[A_0 \sin(\tau) + A_1 \sin(n_1\tau + \phi_1) - l\tau]\} d\tau. \quad (18)$$

If $\phi_1 = 0$, $\mathcal{A}_\mathbf{e}^{(l)}$ is real, while without this condition, this is not guaranteed. Therefore, to set the d-h creation term in the leading order to zero ($\mathcal{B}^{(0)} = 0$), $\phi_1 = 0$ is favorable, and we will focus on this case in the following. Let us introduce the function

$$F^{(1)}[A_0, A_1, n_1, l]$$
$$= \frac{1}{2\pi} \int_0^{2\pi} \cos[A_0 \sin(\tau) + A_1 \sin(n_1\tau) - l\tau] d\tau, \quad (19)$$

with $\mathcal{A}_\mathbf{e}^{(l)} = F^{(1)}[A_0, A_1, n_1, l]$. Then $\mathcal{B}_\mathbf{e}^{(0)} = \mathcal{B}_{-\mathbf{e}}^{(0)} = 0$ is equivalent to $F^{(1)}[A_0, A_1, n_1, -l_0] = F^{(1)}[-A_0, -A_1, n_1, -l_0] = 0$. To realize this, $n_1 = $ odd is favorable since

$$F^{(1)}[-A_0, -A_1, n_1, l] = F^{(1)}[A_0, A_1, n_1, -l]$$
$$= F^{(1)}[A_0, (-)^{n_1+1}A_1, n_1, l](-)^l. \quad (20)$$

Intuitively, this condition can be associated with a parity argument. The auxiliary field A_1 provides additional excitation pathways at the energy of $n_1\Omega$. This is a parity-odd process. On the other hand, the corresponding process using the A_0 field requires n_1 times the absorption of the Ω-frequency electric field excitation. Thus, its parity is $(-)^{n_1}$. Interference between these processes can be expected if n_1 is odd. Otherwise, the excitations involving these two processes end up with different final states.

Since we have only one auxiliary field, the condition which sets $\mathcal{B}^{(0)}$ to zero determines the parameter of the auxiliary field. We call this condition the *optimal* condition for the type-1 protocol. Still, we note that it is not guaranteed that this protocol indeed produces the smallest heating because of the contributions from other processes mentioned in the previous section. In Fig. 3, we illustrate how the coefficients of the effective model scale as a function of A_1. Here, we take $A_0 = -1$, $n_1 = 3$, and $l_0 = 3$, which corresponds to the 3Ω absorption process, and we mainly discuss this case in the
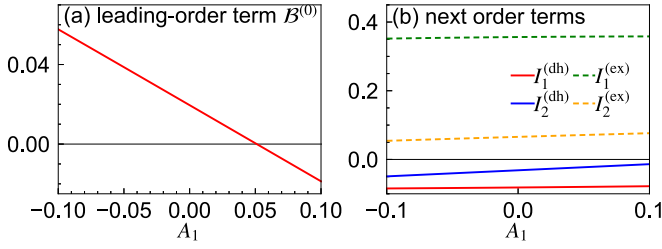
FIG. 3. (a) The coefficient of the doublon-holon creation/annihilation term in the leading-order Floquet Hamiltonian, i.e., $\mathcal{B}_{\mathbf{e}}^{(0)} = F^{(1)}[A_0, A_1, n_1, -l_0]$, as a function of A_1 for the type-1 protocol. (b) The coefficients of the next-order terms in the Floquet Hamiltonian as a function of A_1 for the type-1 protocol. Here, we use $A_0 = -1$, $n_1 = 3$, and $l_0 = 3$.

following sections. One can see that, to minimize $|\mathcal{B}^{(0)}|$, $|A_1|$ much smaller than A_0 is sufficient. In the perturbative regime with respect to the field strength, $\mathcal{B}^{(0)}$ scales as $O(A_0^{l_0})$ for the type-0 excitation. To cancel this term with A_1, we need $A_1 = O(A_0^{l_0})$. Thus, if A_0 remains close to the perturbative regime, we only need small $|A_1|$ to minimize $|\mathcal{B}^{(0)}|$.

2. Type-2 excitation

In the type-2 protocol, on top of the basic electric field excitation, we consider an auxiliary hopping modulation of the form given in Eq. (4). In this case, we have $\mathcal{A}_{\mathbf{e}}^{(l)} = \mathcal{J}_l(A_0) + \frac{\delta_v}{2}[\exp(i\phi_2)\mathcal{J}_{l-n_2}(A_0) + \exp(-i\phi_2)\mathcal{J}_{l+n_2}(A_0)]$. Here, $\mathcal{J}_l$ is the lth-order Bessel function. If $\phi_2 = 0$, $\mathcal{A}_{\mathbf{e}}^{(l)}$ is real, while for other choices, this is not guaranteed. Therefore, to make $\mathcal{B}_{\mathbf{e}}^{(0)} = \mathcal{B}_{-\mathbf{e}}^{(0)} = 0$, $\phi_2 = 0$ is favorable, and we focus on this case in the following. We introduce

$$F^{(2)}[A_0, \delta_v, n_2, l] = \mathcal{J}_l(A_0) + \frac{\delta_v}{2}[\mathcal{J}_{l-n_2}(A_0) + \mathcal{J}_{l+n_2}(A_0)]. \tag{21}$$

Here, $\mathcal{B}^{(0)} = 0$ corresponds to $F^{(2)}[A_0, \delta_v, n_2, -l_0] = F^{(2)}[-A_0, \delta_v, n_2, -l_0] = 0$. For this, $n_2 =$ even is favorable since

$$F^{(2)}[-A_0, \delta_v, n_2, l] = F^{(2)}[A_0, \delta_v, n_2, -l]$$
$$= F^{(2)}[A_0, (-)^{n_2}\delta_v, n_2, l](-)^l. \tag{22}$$

This condition can be associated with a parity argument, as in the case of the type-1 excitation. The only difference is that the hopping process is an even-parity process.

Since we have only one auxiliary field, the condition $\mathcal{B}^{(0)} = 0$ determines the parameter of this auxiliary field. We call this condition the *optimal* condition for the type-2 protocol. In Fig. 4, we illustrate how the coefficients of the effective model scale as a function of A_1. Here, we take $A_0 = -0.6$, $n_2 = 2$, and $l_0 = 2$, which corresponds to the 2Ω absorption process discussed in the following sections. Note that, in the perturbative regime, δ_v for the optimal condition scales as $O(A_0^{n_2})$.

3. Type-3 excitation

In the type-3 protocol, on top of the basic electric field excitation, we consider an auxiliary electric field excitation
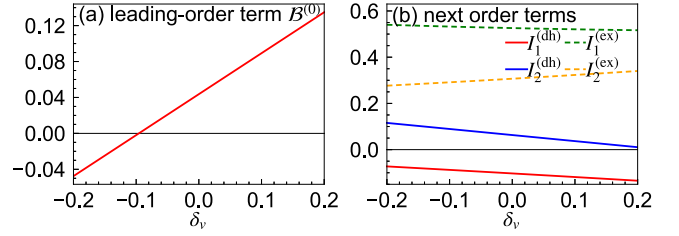
and an auxiliary hopping modulation as defined in Eq. (5). In other words, this protocol is the combination of the type-1 and 2 protocols. Here, we set the phase shifts ϕ_1 and ϕ_2 to zero from the beginning. We introduce

$$F^{(3)}[A_0, A_1, \delta_v, n_1, n_2, l]$$
$$= \frac{1}{2\pi} \int_0^{2\pi} [1 + \delta_v \cos(n_2\tau)]$$
$$\times \exp\{i[A_0 \sin(\tau) + A_1 \sin(n_1\tau)]\}e^{-il\tau}d\tau$$
$$= F^{(1)}[A_0, A_1, n_1, l] + \frac{\delta_v}{2}\{F^{(1)}[A_0, A_1, n_1, l + n_2]$$
$$+ F^{(1)}[A_0, A_1, n_1, l - n_2]\}. \tag{23}$$

Then we have $\mathcal{A}_{\mathbf{e}}^{(l)} = F^{(3)}[A_0, A_1, \delta_v, n_1, n_2, l]$. This function satisfies

$$F^{(3)}[-A_0, -A_1, \delta_v, n_1, n_2, l]$$
$$= F^{(3)}[A_0, A_1, \delta_v, n_1, n_2, -l]$$
$$= F^{(3)}[A_0, (-)^{n_1+1}A_1, (-)^{n_2}\delta_v, n_1, n_2, l](-)^l. \tag{24}$$

Thus, to set the leading-order terms to zero for all bonds, $n_1 =$ odd and $n_2 =$ even are favorable.

In Fig. 5(a), we show $\mathcal{B}^{(0)}$ in the plane of A_1 and δ_v. Here, we use $A_0 = -1$, $n_1 = 3$, $n_2 = 2$, and $l_0 = 3$, which corresponds to the 3Ω absorption process mainly discussed in
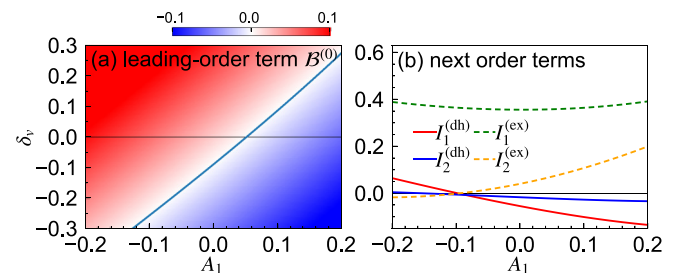

FIG. 4. (a) The coefficient of the doublon-holon creation/annihilation term in the leading-order Floquet Hamiltonian, i.e., $\mathcal{B}_{\mathbf{e}}^{(0)} = F^{(2)}[A_0, \delta_v, n_2, -l_0]$, as a function of δ_v for the type-2 protocol. (b) The coefficients of the next-order terms in the Floquet Hamiltonian as a function of δ_v for the type-2 protocol. Here, we use $A_0 = -0.6$, $n_2 = 2$, and $l_0 = 2$.

FIG. 5. (a) The coefficient of the doublon-holon creation/annihilation term in the leading-order Floquet Hamiltonian, $\mathcal{B}_{\mathbf{e}}^{(0)} = F^{(3)}[A_0, A_1, \delta_v, n_1, n_2, -l_0]$, as a function of A_1 and δ_v for the type-3 protocol. The solid blue line indicates the parameters that correspond to $\mathcal{B}_{\mathbf{e}}^{(0)} = 0$. (b) The coefficients of the next-order terms in the Floquet Hamiltonian as a function of A_1 for the type-3 protocol. We use $A_0 = -1$, $n_1 = 3$, $n_2 = 2$, and $l_0 = 3$.

the following sections. The solid blue line indicates the condition for $\mathcal{B}^{(0)} = 0$. In Fig. 5(b), we show the coefficients of the next-order terms in the Floquet Hamiltonian as a function of A_1 along the $\mathcal{B}^{(0)} = 0$ line in Fig. 5(a). As can be seen, there is a point where both $I_1^{(\mathrm{dh})}$ and $I_2^{(\mathrm{dh})}$ are suppressed, although they are not exactly zero. We choose the condition that minimizes $|I_1^{(\mathrm{dh})}|^2 + |I_2^{(\mathrm{dh})}|^2$ as the *optimal* condition for the type-3 protocol.

III. RESULTS

A. General remarks

In this section, we analyze how well the suppression of heating with multicolor excitations works for the one-band Hubbard model. To this end, we simulate the time evolution of the system under periodic excitations using nonequilibrium DMFT [37,38], which becomes reliable in the limit of high spatial dimensions, using the noncrossing approximation as the impurity solver [47]. Our implementation is based on the open-source library NESSi [48]. To reduce the computational cost of the simulations and enable systematic analyses, we consider the Bethe lattice in the following. We set the bandwidth of the free particle ($U = 0$) problem to $W = 4$ and the interaction $|U| = 15$. Note that we mainly focus on subgap excitations, i.e., Ω is smaller than the gap. The interaction is chosen such that, near the resonance condition $|U| = 3\Omega$ ($|U| = 2\Omega$), there are no other relevant absorption processes with $l\Omega \neq 3\Omega$ ($l\Omega \neq 2\Omega$) but that Ω is reasonably small under this condition. In the Bethe lattice, the effects of the electric field can be taken into account by considering two types of bonds connected to the effective impurity site, which are parallel and antiparallel to the external field, respectively. This treatment mimics the electric field applied to the body-diagonal direction in hypercubic lattices. Since the technical aspects have been discussed in previous works [49–52], we skip the details here. In Appendix A, we show the results for the system on the two-dimensional (2D) square lattice and confirm that the Bethe lattice and the 2D square lattice produce the qualitatively same results.
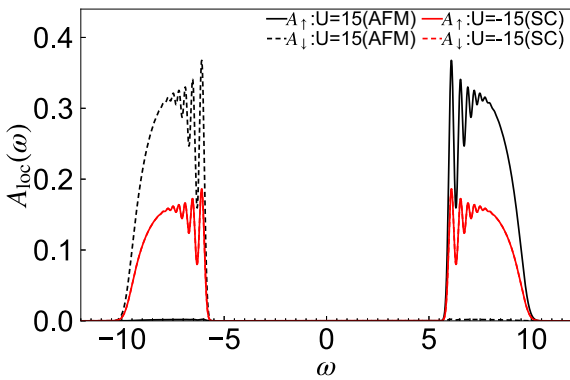

FIG. 6. Local single-particle spectral functions for $U = 15$ and $U = -15$ in equilibrium at $T = 0.02$. For $U = 15$, the system is in an antiferromagnetic (AFM) state with spins aligned along the z direction. For $U = -15$, the system is in a superconducting (SC) state with a real order parameter. The red solid and dashed lines overlap.
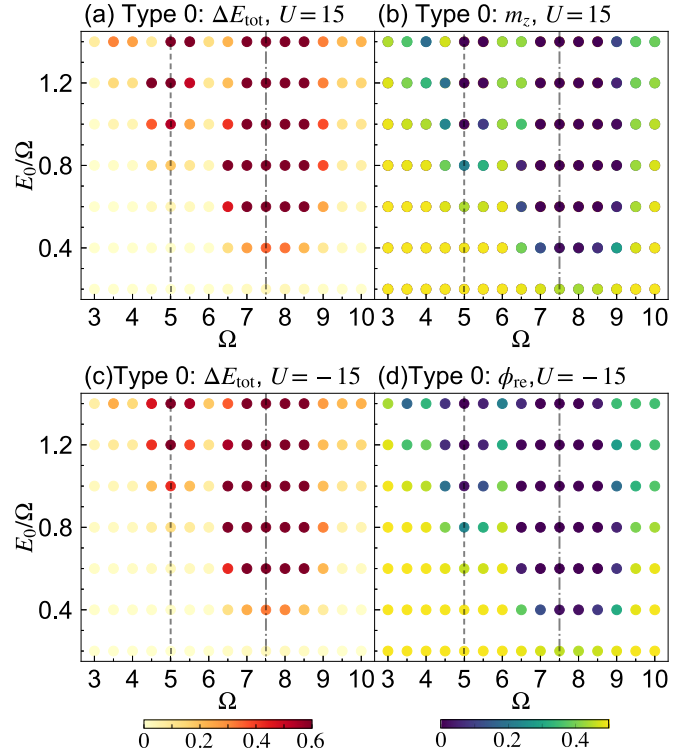

FIG. 7. The difference of the total energy from its equilibrium value (ΔE_{tot}) and the value of the order parameter (m_z or ϕ_{re}) in the plane of the excitation frequency Ω and the field strength E_0/Ω ($= -A_0$). These physical quantities are averaged over a time interval $2\pi/\Omega$ around $t = 50$, the type-0 excitation is used, and the initial temperature is $T = 0.02$. (a) and (b) show results for $U = 15$, where the initial state is an antiferromagnetic state with spins aligned along the z direction. (c) and (d) show results for $U = -15$, where the initial state is a superconducting state with real order parameter. The vertical dashed lines indicate $\Omega = |U|/3$ and the vertical dot-dashed lines indicate $\Omega = |U|/2$.

B. Equilibrium state at $t = 0$

One of the major goals of Floquet engineering is to control the low-energy physics. Thus, we choose as initial equilibrium states at $t = 0$ ordered states and see how the order evolves under external fields at $t > 0$. In practice, we use $U = 15$ or -15 and set the initial temperature low enough ($T = 0.02$), so that the corresponding order parameters are almost saturated. For $U = 15$, the initial state is in the antiferromagnetic (AFM) phase, with spins ordered along the z direction. The corresponding order parameter is $m_z(t) = \frac{1}{2}\langle \hat{n}_{i\uparrow}(t) - \hat{n}_{i\downarrow}(t)\rangle$. For $U = -15$, we choose the initial state in the superconducting (SC) phase with real order parameter $\phi_{\mathrm{re}}(t) = \mathrm{Re}\langle \hat{c}_{i\uparrow}^{\dagger}(t)\hat{c}_{i\downarrow}^{\dagger}(t)\rangle$. In Fig. 6, we show the local single-particle spectral functions of these states. We plot $A_\sigma(\omega) = -\frac{1}{\pi}\mathrm{Im}G_\sigma^R(\omega)$, where $G_\sigma^R(\omega)$ is the Fourier transform of $G_\sigma^R(t) \equiv -i\theta(t)\langle[\hat{c}_{i,\sigma}(t), \hat{c}_{i,\sigma}^{\dagger}(0)]_+\rangle$. Here, $\theta(t)$ is the Heaviside function, and $[,]_+$ indicates the anticommutator. In both cases, the band gap is ~ 11, while the separation between the bottom of the lower band and the top of the upper band is ~ 20. The peak structures in the upper and lower Hubbard bands in the AFM phase correspond to spin polarons which appear due to the spin-charge coupling in this system [53–55]. Since the
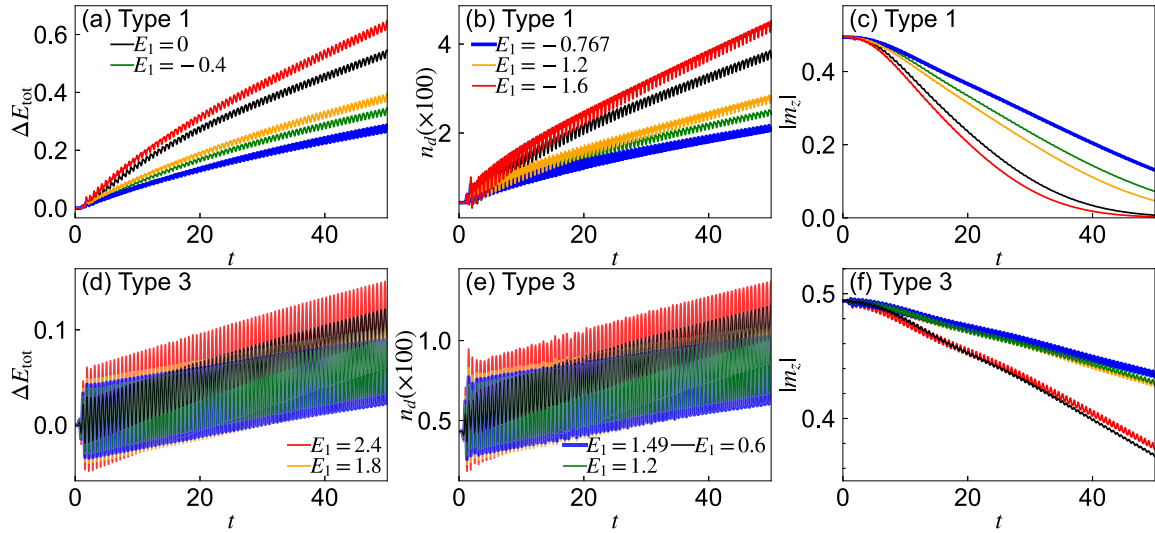
FIG. 8. (a,d) Evolution of the difference of the total energy from its equilibrium value ΔE_{tot}, (b,e) that of the number of doublons n_d, and (c,f) that of the staggered magnetization m_z under periodic excitations with $\Omega = U/3$. Here, we set $U = 15$ and the initial temperature to $T = 0.02$, where the initial state is antiferromagnetically ordered with spins aligned along the z direction. The parameters of the main electric field excitation are $\Omega = 5$ and $A_0 = -1$ ($E_0 = 5$). For (a)–(c), we use the type-1 protocol with $l_0 = 3$ and $n_1 = 3$. These panels share the legend, which indicates the values of the auxiliary electric field. For (d)–(f), we use the type-3 protocol with $l_0 = 3$, $n_1 = 3$, and $n_2 = 2$, and the strength of the auxiliary electric field and hopping modulation is chosen such that the doublon-holon creation term vanishes in the leading order. These panels share the legend, and the parameters of the auxiliary fields are $(E_1, \delta_v) = (0.6, -0.157)$, $(1.2, -0.223)$, $(1.49, -0.255)$, $(1.8, 0.289)$, $(2.4, -0.354)$, but only the values of the auxiliary electric field are shown. The thick blue lines correspond to the optimal conditions for each protocol, as predicted by the Floquet Hamiltonian.

AFM phase for $U > 0$ and the SC phase for $U < 0$ are related by a particle-hole transformation (Shiba transformation), there are corresponding structures also in the spectrum of the SC phase.

C. Suppression of heating

Now we apply the external fields to the abovementioned initial states. In practice, we multiply the time periodic expressions for $\delta v(t)$ and $A(t)$, i.e., Eqs. (2)–(5), by an envelope function $F(t; t_r)$ to smoothly switch the Hamiltonian from the equilibrium one to the time-periodic one within a time t_r. The specific form of the ramp function is $F(t; t_r) = \theta(t_r - t)[\frac{1}{2} - \frac{3}{4} \cos(\pi t/t_r) + \frac{1}{4} \cos(\pi t/t_r)^3] + \theta(t - t_r)$, and we set $t_r = 2$. Note that our choice of t_r is short enough that it does not qualitatively affect the discussion below, which focuses on the dynamics under periodic excitations.

First, we show how the total energy and the order parameters evolve without auxiliary excitations. In Fig. 7, we show the difference of the total energy from its equilibrium value and the order parameters averaged around $t = 50$ in the plane of the frequency Ω and the excitation strength E_0/Ω ($= -A_0$). Without excitations, the values of the order parameters are ~0.5. In both the repulsive and attractive cases, the total energy resonantly increases around $|U| \simeq 3\Omega$ and 2Ω, and accordingly, the order parameters are reduced substantially. The strong heating and melting of the order are caused by 3Ω and 2Ω absorption processes. Our goal is to suppress these absorption processes with auxiliary excitations.

1. Suppression of 3Ω absorption

We focus first on the 3Ω absorption and consider the excitation protocols with $l_0 = \pm 3$, $n_1 = 3$, and $n_2 = 2$. In Fig. 8,

we show the evolution of the difference of the total energy from its equilibrium value ΔE_{tot}, that of the number of doublons $n_d = \langle \hat{n}_{i\uparrow} \hat{n}_{i\downarrow} \rangle$, and that of the staggered magnetization m_z for the type-1 and 3 protocols. Here, we set $U = 15$, $\Omega = 5$, and $E_0 = 5$. In Fig. 9, we plot n_d and m_z averaged around $t = 50$ as a function of the strength of the auxiliary electric field E_1 for the type-1 and 3 protocols. In the case of the type-1 protocol, the increase of ΔE_{tot} and n_d as well as the melting of the AFM order become slowest when the condition for $\mathcal{B}^{(0)} = 0$ is met, i.e., for the optimal condition for the type-1 protocol. Remember that we set the phase of the auxiliary field ϕ_1 to zero. We numerically confirmed that the heating and melting of the order become stronger with nonzero ϕ_1 (not shown), as we expected in Sec. II D 1.

On the other hand, for the type-3 protocol, we change the parameters such that $\mathcal{B}^{(0)} = 0$ is always satisfied. The results show that the increase of ΔE_{tot} and n_d and the melting of the AFM order become slowest when the next-order d-h creation terms of the Floquet Hamiltonian are strongly suppressed, i.e., for the optimal condition for the type-3 protocol. In both protocols, ΔE_{tot} and n_d behave similarly, which indicates that, in the present large-U regime, the dominant heating process is the d-h creation. The renormalization of the single-particle spectrum caused by the excitations is discussed in Appendix D. The attractive model also shows the same behavior as Figs. 8 and 9. Note that, for the present parameters, the coefficients of the d-h creation terms in the leading and the next-leading order are comparable, see Fig. 3. The success of the strategy of suppressing these terms order by order indicates that there is no significant interference between the processes described by the different terms in the effective Hamiltonian. Also, the change in the coefficients of
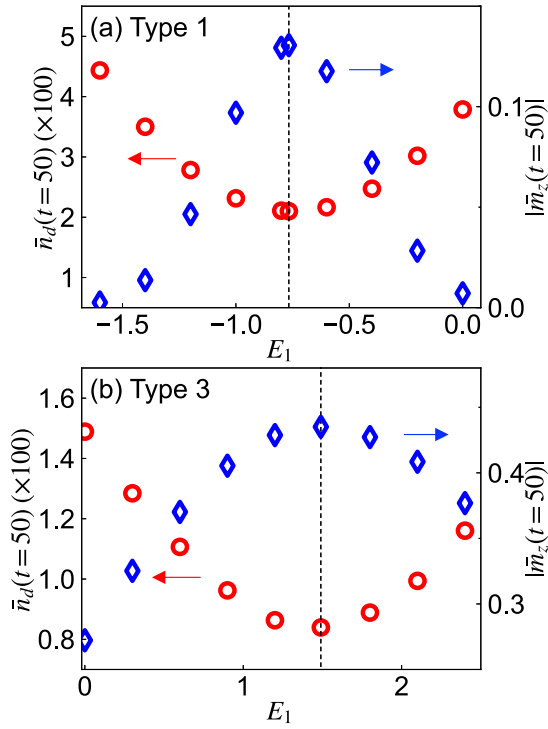
FIG. 9. Number of doublons and staggered magnetization averaged over a time interval $\frac{2\pi}{\Omega}$ around $t = 50$ as a function of the strength of the auxiliary electric field (E_1). We set $U = 15$ and the initial temperature to $T = 0.02$, where the initial state is antiferromagnetic. The parameters of the main electric field excitation are $\Omega = 5$ and $A_0 = -1$. For (a), we use the type-1 protocol with $l_0 = 3$ and $n_1 = 3$. For (b), we use the type-3 protocol with $l_0 = 3$, $n_1 = 3$, and $n_2 = 2$, and the strength of the auxiliary electric field and hopping modulation is chosen such that the doublon-holon creation term vanishes in the leading order. The dashed lines indicate the optimal conditions for each protocol.

the d-h creation terms of higher orders should be moderate when we adjust the auxiliary field to suppress the low-order terms.

Let us note that a similar suppression of heating by multicolor driving is also observed for even larger U, see Appendix C. It can be well explained by the Floquet Hamiltonian how physical quantities for each protocol scale with U. The fact that the Floquet Hamiltonian provides a good description indicates that the observed heating process can be associated with the Floquet prethermalization process [45,56]. Higher-order processes are expected to drive the system toward the infinite temperature state on longer time scales, where the description based on the Floquet Hamiltonian is no longer valid [56].

In Figs. 10(a) and 10(b), we compare the evolution of the order parameters for the type-0 excitation, the optimal type-1 excitation, and the optimal type-3 excitation. Here, we also show the results for the optimal type-2 excitation for completeness. The optimal type-1 and 2 excitations can be regarded as unoptimized cases for the type-3 excitation. Although the effect of the auxiliary drive depends on the order, with the type-3 excitation, melting of the order is strongly suppressed both in the repulsive and attractive models. We also note that, for the type-2 excitation, one finds that the
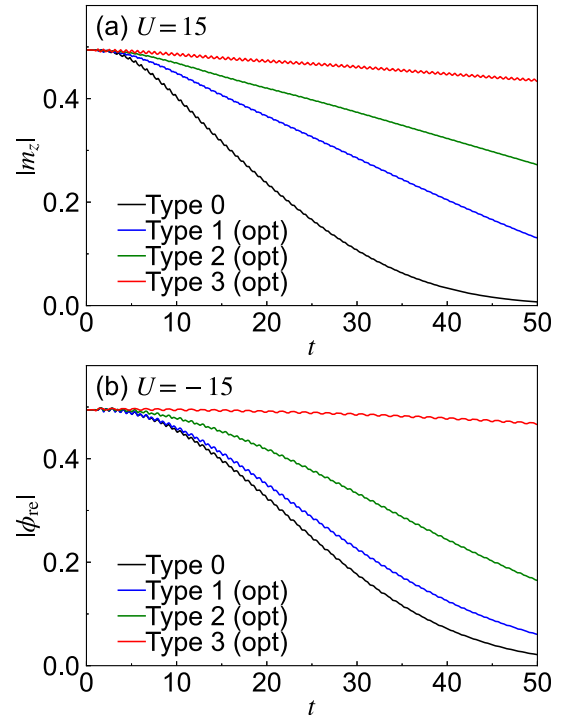

FIG. 10. Time evolution of the order parameters under the type-0, 1, 2, and 3 protocols with optimal parameters. Here, $l_0 = \pm 3$, $n_1 = 3$, and $n_2 = 2$. In panel (a), the system parameters and excitation conditions are the same as in Fig. 8. In panel (b), the excitation conditions are the same as in (a), but we use $U = -15$ and choose as the initial state the superconducting state with real order parameter at $T = 0.02$.

optimal condition predicted by the Floquet Hamiltonian ($\delta_v = -0.0889$ in the case of Fig. 10) indeed leads to an efficient suppression of heating both for the AFM and SC phases. However, for the SC phase, it turns out that heating can be further suppressed by decreasing δ_v from -0.0889 (not shown). This may be because both $I_1^{(dh)}$ and $I_2^{(dh)}$ are further reduced simultaneously, unlike in the case of the type-1 protocol, see Fig. 3.

In Fig. 11, we compare the values of order parameters averaged around $t = 50$ obtained by the type-0 and 3 protocols. For the type-3 calculations, the optimal parameters are used. Around $\Omega = 5$, the melting of the order is strongly suppressed by the auxiliary drives for both $U = 15$ and -15, which can be attributed to the suppression of the 3Ω absorption, as discussed above. Around $\Omega = 6$–8, one can also observe a slower melting. However, in this regime, 2Ω absorption can also happen. To fully discuss the conditions for the suppression of the 2Ω absorption, one needs to consider the effective model in the $\pm 2\Omega$ rotating frame. Around $\Omega = 4$, the melting speed is increased, which may be attributed to the enhancement of the 4Ω absorption processes by the auxiliary excitations.

We note that the behavior of the total energy is almost the same as that of the order parameter (not shown). More specifically, the suppression of the order parameters is accompanied by an increase of the total energy. These results demonstrate that the Floquet Hamiltonian for a given rotating frame serves as a useful guide for protocols which
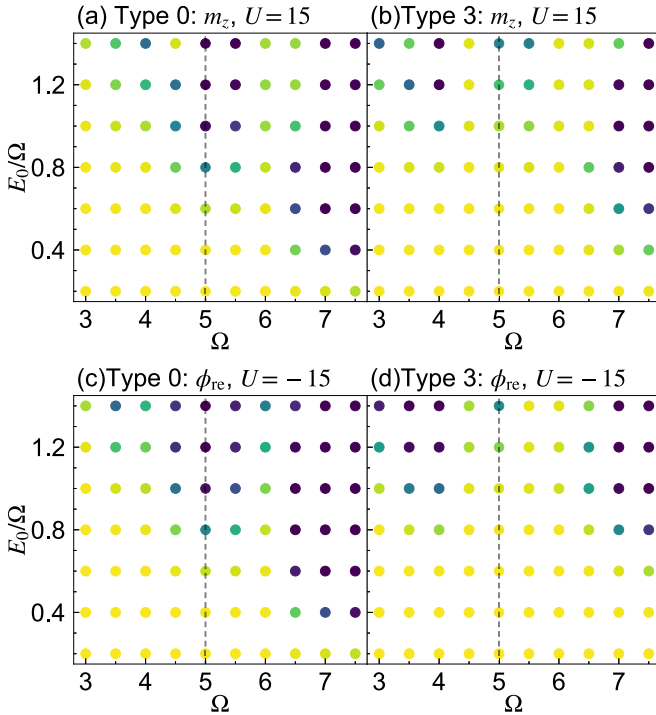
FIG. 11. The value of the order parameters (m_z or ϕ_{re}) averaged around $t = 50$ for (a,b) $U = 15$ and (c,d) $U = -15$ in the plane of the excitation frequency Ω and the field strength E_0/Ω ($= -A_0$). We focus on the regime around $|U| = 3\Omega$. In panels (a) and (c), the type-0 excitation is used, while in (b) and (d), the type-3 excitation with the optimal parameters for $l_0 = \pm 3$, $n_1 = 3$, and $n_2 = 2$ is used. The vertical dashed lines indicate $\Omega = |U|/3$. The other conditions and the color code are the same as in Fig. 7.

suppress the corresponding absorption via multicolor excitations, but auxiliary excitations can both suppress or enhance other absorptions.

2. Suppression of 2Ω absorption

Next, we try to suppress the 2Ω absorption using the type-2 protocol with $l_0 = \pm 2$ and $n_2 = 2$. In Fig. 12, we show the evolution of the order parameters and the deviation of the total energy from its equilibrium value, both for $U > 0$ and $U < 0$ and for the indicated values of δ_v. Here, we use $|U| = 15$, $\Omega = 7.5$, and $A_0 = -0.6$. The rate of increase in the total energy and the speed of melting of the order parameters are slowest when the leading-order d-h creation terms become zero, i.e., when $\mathcal{B}^{(0)} = 0$.

The suppression of heating is more effective for the SC phase than for the AFM phase. We note that the next leading d-h creation/annihilation terms remain nonzero in the optimal condition, see Fig. 4. The difference between AFM and SC should be attributed to how these terms act on the different ordered phases. Remember that we set the phase of the auxiliary field ϕ_2 to zero. We numerically confirmed that the heating and melting of the orders becomes stronger with nonzero ϕ_2 (not shown), as we expected in Sec. II D 2.

We summarize the results in Fig. 13, where we compare the values of order parameters at $t = 50$ around $|U| \simeq 2\Omega$ between the type-0 protocol and the type-2 protocol with
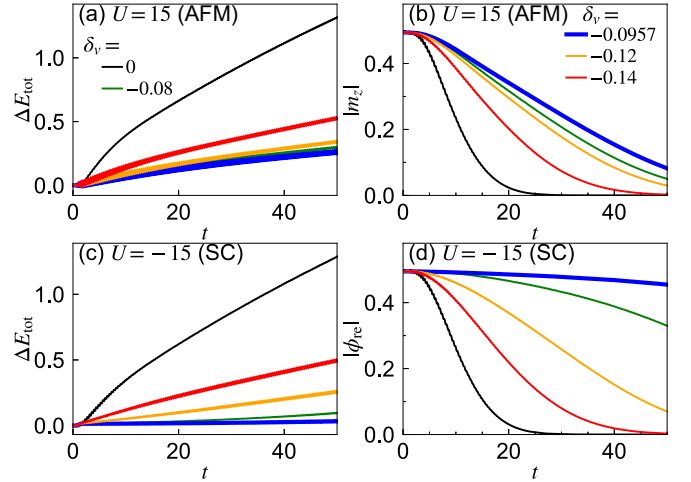

FIG. 12. (a,c) Time evolution of the deviation of the total energy from its equilibrium value ΔE_{tot} and (b,d) that of the order parameters for type-2 protocols with $l_0 = \pm 2$, $n_2 = 2$, and the indicated values of δ_v. The parameters of the main drive are $\Omega = 7.5$ and $A_0 = -0.6$ ($E_0 = 4.5$). All panels share the legend. In (a) and (b), we set $U = 15$ and the initial temperature to $T = 0.02$, so that the initial state is antiferromagnetic (AFM) with spins aligned along the z direction. In (c) and (d), we set $U = -15$ and the initial temperature to $T = 0.02$, where the initial state is a superconducting (SC) state with real order parameter. The thick blue lines correspond to the optimal conditions predicted by the Floquet Hamiltonian.
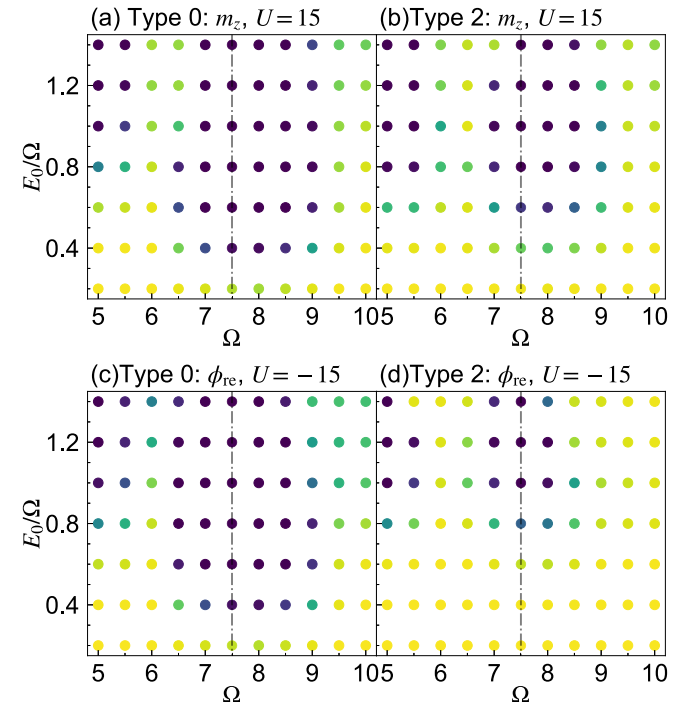

FIG. 13. The values of the order parameters (m_z or ϕ_{re}) averaged around $t = 50$ for (a,b) $U = 15$ and (c,d) $U = -15$ in the plane of the excitation frequency Ω and the field strength E_0/Ω ($= -A_0$). We focus on the regime around $|U| = 2\Omega$. In panels (a) and (c), the type-0 excitation is used, while in (b) and (d), the type-2 excitation with the optimal parameters for $l_0 = \pm 2$ and $n_2 = 2$ is used. The vertical dot-dashed lines indicate $\Omega = |U|/2$. The other conditions and the color code are the same as in Fig. 7.

the optimal parameters. For both $U = 15$ and -15, the 2Ω absorption is suppressed. As expected from Fig. 12, the suppression is strong for $U < 0$ (the SC phase). In addition, we checked that the behavior of the total energy is almost the same as that of the order parameter (not shown).

D. Extraction of exchange couplings

In this section, we illustrate how the suppression of heating helps us to observe the modification of the low-energy physics due to the virtual excitations induced by the periodic excitations. In the present systems, this low-energy physics is characterized by the exchange couplings between the spins or pseudospins in the repulsive and attractive regimes, respectively. As discussed in previous works [16,57], one way to measure the exchange couplings is to compare the (pseudo-)spin dynamics obtained from DMFT with the mean-field (MF) dynamics of the Heisenberg (XXZ) spin models, i.e., the solution of a Landau-Lifshitz (LL) equation.

We first discuss how the measurement of the exchange coupling works for repulsive U. Note that the periodic excitation does not break the SU(2) symmetry. When the exchange coupling is modified by the periodic excitations, a spin precession occurs if we additionally apply a homogeneous magnetic field. If we assume that the homogeneous magnetic field is applied along the x direction, the spin model can be written as $\hat{H}_{\text{spin}}(t) = J_{\text{ex}}(t)\sum_{(i,j)}\hat{\mathbf{s}}_i\hat{\mathbf{s}}_j + B_x\mathbf{e}_x\sum_i\hat{\mathbf{s}}_i$. The MF Hamiltonian becomes $\hat{H}_{\text{spin}}^{\text{MF}} = \sum_i \mathbf{B}_i^{\text{eff}}\hat{\mathbf{s}}_i$, where $\mathbf{B}_i^{\text{eff}} = J_{\text{ex}}(t)\sum_{\delta}\mathbf{s}_{i+\delta}(t) + B_x\mathbf{e}_x$. Here, $\mathbf{s}(t)$ is the expectation value of $\hat{\mathbf{s}}$, and δ indicates the neighboring sites. Then the corresponding LL equation becomes $\partial_t\mathbf{s}_i(t) = \mathbf{B}_i^{\text{eff}}(t) \times \mathbf{s}_i(t)$. In the present case, we have the relation $s_{A,y,z} = -s_{B,y,z}$ and $s_{A,x} = s_{B,x}$ (A and B are sublattice indices). From this, we obtain

$$ZJ_{\text{ex}} = -\frac{B_0}{2s_x} - \frac{\dot{s}_y}{2s_xs_z}. \tag{25}$$

Here, $\dot{s}_y$ is the time derivative, Z is the number of neighboring sites, and we omit the time indices. In the previous works, this equation has been used to discuss the effects of photodoping [57] or periodic excitations on the exchange interactions [16]. In this paper, we apply the above formula to the time-averaged values of $\mathbf{s}(t)$, $\bar{\mathbf{s}}(t) \equiv \frac{1}{T_p}\int_{t-T_p/2}^{t+T_p/2}\mathbf{s}(t)dt$, where $T_p = \frac{2\pi}{\Omega}$, to eliminate effects related to the micromotion.

In Fig. 14(a), we show the resultant values of $J_{\text{ex}}(t)$ for different excitation protocols for $U = 15$, $\Omega = 5$, and $A_0 = -1$. For this parameter set, the Floquet Hamiltonian produces an enhanced $J_{\text{ex}}(t)$ compared with the equilibrium value, due to the virtual excitations associated with the periodic excitations. For the type-0 protocol, the value initially matches $J_s^{\text{(HE)}}$, but $J_{\text{ex}}(t)$ gradually decreases with time. For the type-1 protocol, the tendency is the same, but the deviation from the expected exchange coupling is less severe. For the type-3 protocol, $J_{\text{ex}}(t)$ remains close to the expected coupling within the time range studied here. The deviation from the expected value can be attributed to the photodoping. In Ref. [57], it was pointed out that photodoping effectively reduces J_{ex}, like chemical doping. This behavior can be intuitively understood since the doping reduces the number of singly occupied sites, so that
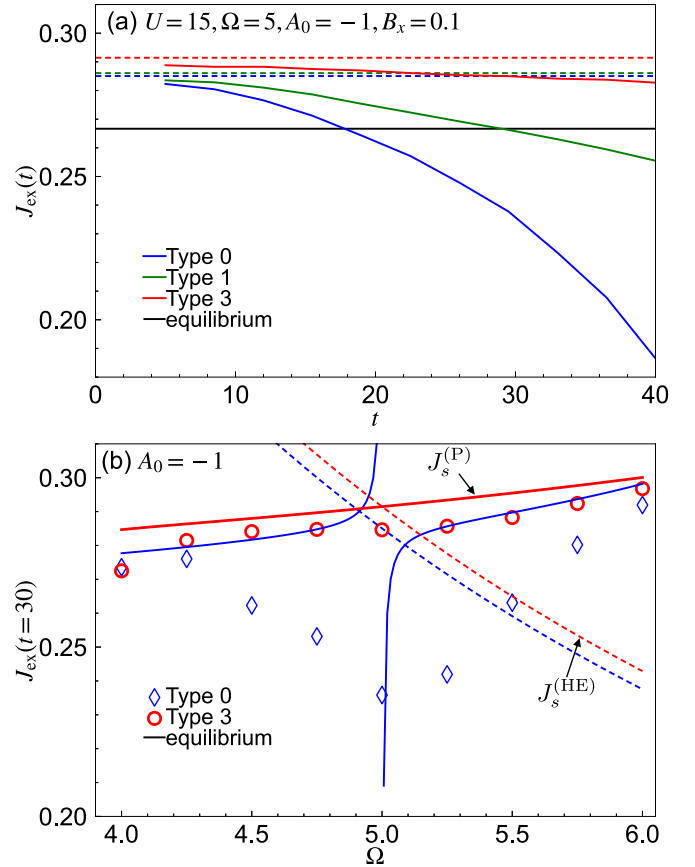

FIG. 14. (a) Time evolution of the exchange coupling evaluated from Eq. (25) for $U = 15$, $\Omega = 5$, $A_0 = -1$, and $B_x = 0.1$. The dashed lines indicate $J_s^{\text{(HE)}}$ [Eq. (13)], while the solid black line indicates the equilibrium value of the exchange coupling. Here, we set $l_0 = n_1 = 3$ and $n_2 = 2$. (b) The estimated exchange couplings as a function of Ω at $t = 30$ for $U = 15$, $A_0 = -1$, and $B_x = 0.1$. Here, the type-3 excitation with the optimal parameters for $l_0 = n_1 = 3$ and $n_2 = 2$ is used. The dashed lines show $J_s^{\text{(HE)}}$ [Eq. (13)], while colored solid curves show $J_s^{\text{(P)}}$ [Eq. (16)].

the probability of finding spins on neighboring sites which develop correlations is reduced [58]. With the type-0 protocol, as time evolves, more particles are excited across the gap to reduce J_{ex}, which competes with the effects of the virtual excitations. The undesired photodoping (absorption) can be suppressed with the type-1 and 3 protocols.

To summarize, in Fig. 14(b), we show how the estimated J_{ex} behaves at $t = 30$ near the $U = 3\Omega$ resonance. Let us first discuss the behavior of the type-0 protocol. For this protocol, the prediction from perturbation theory $J_{\text{ex}}^{\text{(P)}}$ shows a divergence at $U = 3\Omega$ due to the virtual fluctuations to the 3Ω-dressed states, while the prediction from the high-frequency expansion $J_{\text{ex}}^{\text{(HE)}}$ is regular since the contribution from such states is not included. However, both fail to explain the actual behavior of J_{ex}, which is strongly suppressed near the resonance $U = 3\Omega$. This can be attributed to the strong enhancement of the density of photocarriers in this regime, which is neither considered in $J_{\text{ex}}^{\text{(HE)}}$ nor in $J_{\text{ex}}^{\text{(P)}}$. As for the type-3 protocol, J_{ex} is generally larger than the corresponding
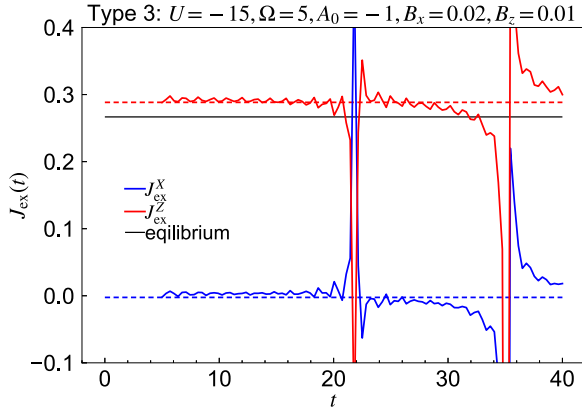
FIG. 15. Time evolution of the exchange coupling evaluated from Eq. (26) for $U = -15$, $\Omega = 5$, $A_0 = -1$, $B_x = 0.02$, and $B_z = 0.01$. Here, the type-3 excitation with the optimal condition for $l_0 = -3$, $n_1 = 3$, and $n_2 = 2$ is used. The dashed lines indicate $J_{\eta,XY}^{(HE)}$ and $J_{\eta,Z}^{(HE)}$ [Eq. (15)].

value for the type-0 protocol. The resonant reduction of J_{ex} around the resonance is absent, and J_{ex} tends to increase with increasing Ω. For the type-3 protocol, $J_{ex}^{(P)}$ is regular as a function of Ω since the diverging term is suppressed due to the condition $\mathcal{B}^{(0)} = 0$. Here, $J_{ex}^{(HE)}$ is also regular. Note that $J_{ex}^{(HE)}$ becomes equal to $J_{ex}^{(P)}$ for the type-3 protocol at $U = 3\Omega$. Importantly, the behavior of the numerically evaluated J_{ex} is well explained by $J_{ex}^{(P)}$ for the type-3 protocol.

Remember that the conditions under which $J_{ex}^{(P)}$ and $J_{ex}^{(HE)}$ are justified are different. Namely, $|U|$, Ω, $|\Delta U| \gg |v_0|$ is required for $J_{ex}^{(P)}$, while $|U|$, $\Omega \gg |v_0|$, $|\Delta U|$ is required for $J_{ex}^{(HE)}$. The results show that, under the condition that heating is well suppressed, $J_{ex}^{(P)}$ describes the low-energy physics better than $J_{ex}^{(HE)}$ in practice. The qualitative difference between the Ω dependence of $J_{ex}^{(HE)}$ and $J_{ex}^{(P)}$ can be attributed to additional contributions from the ΔU term in the denominator in $J_{ex}^{(P)}$, which are absent in $J_{ex}^{(HE)}$.

As in the case of the AFM phase for $U > 0$, one can measure the modified exchange couplings of the pseudospins for $U < 0$ by comparing the DMFT results with the MF dynamics of the pseudospins: $\hat{H}_{\eta\text{-spin}}(t) = J_{\eta,XY}(t) \sum_{\langle ij \rangle}(\hat{\eta}_i^x \hat{\eta}_j^x + \hat{\eta}_i^y \hat{\eta}_j^y) + J_{\eta,Z}(t) \sum_{\langle ij \rangle} \hat{\eta}_i^z \hat{\eta}_j^z + B_x \sum_i (-)^i \eta_i^x + B_z \sum_i (-)^i \eta_i^z$. Physically, the B_x term corresponds to a homogeneous pair potential [remember the $(-)^i$ factor in the definition of $\hat{\eta}_i^x$], which favors the development of the real SC order parameter. The B_z term corresponds to a staggered potential, which favors the development of charge order. As in the case of $U > 0$, one can consider the MF dynamics of this system, which yields

$$ZJ_X = \frac{1}{2}\left[\frac{B_x}{\eta_x} + \frac{\dot{\eta}_x}{\eta_y \eta_z} - \frac{\dot{\eta}_y}{\eta_x \eta_z}\right], \quad (26a)$$

$$ZJ_Z = \frac{1}{2}\left[\frac{2B_z}{\eta_z} - \frac{B_x}{\eta_x} + \frac{\dot{\eta}_x}{\eta_y \eta_z} + \frac{\dot{\eta}_y}{\eta_x \eta_z}\right]. \quad (26b)$$

In Fig. 15, we show the exchange couplings estimated from these equations for the type-3 protocol with optimal parameters for $U = -15$, $\Omega = 5$, and $A_0 = -1$. One can see that the measured J_X and J_Z match the predictions for $J_{\eta,X}^{(HE)} (=$

$J_{\eta,X}^{(P)})$ and $J_{\eta,Z}^{(HE)} (= J_{\eta,Z}^{(P)})$ well. Still, at some times, strong deviations from the predicted values are observed because η^y becomes small for these times. We note that, with other excitation protocols, the deviations from the expected values are severe, which can again be attributed to the effect of photodoping.

IV. CONCLUSIONS

In this paper, we showed that heating, which is a typically undesired side effect of Floquet engineering, can be significantly suppressed using multicolor excitation protocols and interference between different excitation pathways in strongly correlated system. We focused on the one-band Hubbard model and considered subgap but strong electric field excitations with frequency Ω as the main drive. As auxiliary excitations, we discussed additional electric field excitations and/or hopping modulations with frequencies corresponding to higher harmonics of Ω. Using nonequilibrium DMFT, which is reliable for high-dimensional systems, we studied how the multicolor excitation protocols suppress heating. We showed that the effective Floquet Hamiltonian in the rotating frame serves as a useful guide in determining the conditions for the efficient suppression, focusing on 3Ω- and 2Ω-absorption processes. In practice, an efficient suppression can be realized by suppressing the d-h creation terms in the Floquet Hamiltonian order by order. We also measured the evolution of the exchange couplings in the driven systems and demonstrated that the suppression of heating removes potentially competing effects associated with photodoping. Multicolor driving protocols thus allow to more clearly observe the modifications of the low-energy physics resulting from virtual excitations and hence the desired Floquet engineered properties.

We expect that the physics discussed in this paper can be directly observed in cold-atom experiments [22,31]. An important question is how well the multicolor excitations suppress heating in real materials. The single-band Hubbard model with a large Coulomb interaction can be realized, for example, in alkali-metal-loaded zeolites [59] and alkali-cluster-loaded sodalites [60], where our results may be directly applied. For general strongly correlated systems, further analyses of models with multiple orbitals and different lattice structures are required. Other intriguing issues which may be addressed in the future are the role of the coherence of the excited states and the dimensionality of the system. In this paper, we found that the interference between the excitation processes represented by different terms in the effective Hamiltonian is insignificant in high-dimensional systems described by DMFT. Still, one can expect that such interference effects become important when there are only a few potential final states and the excitations occur before the coherence between the ground state and the excited state is lost. In Mott insulators in dimensions >1, due to the spin-charge coupling, this coherence time is typically short [52]. On the other hand, in lower-dimensional systems, particularly in one dimension, the spin-charge coupling become less important, and the coherence of the excited states lasts longer [61,62]. In such a situation, the interference effects originating from the different terms in the Floquet Hamiltonian can be important.
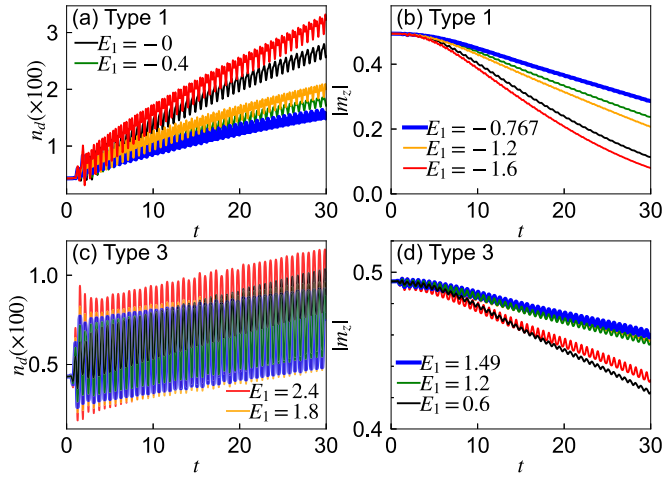
FIG. 16. (a,c) Evolution of the density of doublons n_d and (b,d) the staggered magnetization m_z under periodic excitations with $\Omega = U/3$. Here, we consider the system on the two-dimensional square lattice and set $v_0 = 0.5$ and $U = 15$. The initial temperature is $T = 0.02$, so that the system is initially in the antiferromagnetic phase, with the spins pointing along the z direction. The parameters of the main drive are $\Omega = 5$ and $A_0 = -1$ ($E_0 = 5$). In panels (a) and (b), which share the labels, we use the type-1 protocol with $n_1 = 3$ and the indicated values of the auxiliary electric field. In (c) and (d), which also share the labels, we use the type-3 protocol with $n_1 = 3$ and $n_2 = 2$. The values of the auxiliary electric field and hopping modulations are chosen such that $\mathcal{B}_e^{(0)}$ is zero, i.e., $(E_1, \delta_v) = (0.6, -0.0784), (1.2, -0.112), (1.49, -0.128), (1.8, -0.145), (2.4, -0.177)$. In the figure, only the values of the auxiliary electric field are shown. The thick blue lines correspond to the optimal parameters for each protocol as predicted by the Floquet Hamiltonian.

ACKNOWLEDGMENTS

APPENDIX A: RESULTS FOR THE 2D SQUARE LATTICE

In this section, we show supplementary DMFT results for the Hubbard model on the 2D square lattice. Compared with the case of the Bethe lattice, simulations for the 2D square lattice require more computational resources since one needs to deal with momentum-dependent Green's functions. Thus, it is more difficult to make systematic analyses as we did for the Bethe lattice in the main text. Still, by comparing some cases, we confirm that the 2D square lattice and the Bethe lattice yield qualitatively the same results.

Here, we set the hopping parameter to $v_0 = 0.5$, so that the bandwidth of the free system ($U = 0$) is 4 as in the case of the Bethe lattice. We consider the field applied to the diagonal of the square lattice. In Fig. 16, we show the evolution of the double occupation $n_d(t)$ and the AFM order parameter $m_z(t)$ for $U = 15$, $\Omega = 5$, and $A_0 = -1$. These results can be directly compared with those in Fig. 8 for the Bethe lattice,

and they show the qualitatively same behavior. We observe the strongest suppression of heating for the optimal condition predicted by the Floquet Hamiltonian.

APPENDIX B: EXPRESSIONS FOR $\hat{H}_{\text{eff}}^{(2)}$

In this section, we present the explicit expressions for $\hat{H}_{\text{eff},2}^{(2)}$ and $\hat{H}_{\text{eff},3}^{(2)}$. For $\hat{H}_{\text{eff},2}^{(2)}$, we need to evaluate $[\hat{g}_{ij\sigma}, \hat{h}_{i'j'\sigma'}^{\dagger}]$, which can be expressed as follows:

(1) $i' = i$, $j' = j$: 0
(2) $i' = j$, $j' = i$: 0
(3) $i' = i$, $j' \neq j$
  (a) $\sigma' = \sigma$: 0
  (b) $\sigma' = \bar{\sigma}$: $-c_{i\sigma}^{\dagger} c_{j\sigma} c_{i\bar{\sigma}}^{\dagger} c_{j'\bar{\sigma}} \bar{n}_{j\bar{\sigma}} \bar{n}_{j'\sigma}$
(4) $i' \neq i$, $j' = j$
  (a) $\sigma' = \sigma$: 0
  (b) $\sigma' = \bar{\sigma}$: $-c_{i\sigma}^{\dagger} c_{j\sigma} c_{i'\bar{\sigma}}^{\dagger} c_{j\bar{\sigma}} n_{i\bar{\sigma}} n_{i'\sigma}$
(5) $i' = j$, $j' \neq i$
  (a) $\sigma' = \sigma$: $c_{i\sigma}^{\dagger} c_{j'\sigma} n_{i\bar{\sigma}} n_{j\bar{\sigma}} \bar{n}_{j'\bar{\sigma}}$
  (b) $\sigma' = \bar{\sigma}$: $c_{j\bar{\sigma}}^{\dagger} c_{j'\bar{\sigma}} c_{i\sigma}^{\dagger} c_{j\sigma} \bar{n}_{j'\sigma} n_{i\bar{\sigma}}$
(6) $i' \neq j$, $j' = i$
  (a) $\sigma' = \sigma$: $-c_{i'\sigma}^{\dagger} c_{j\sigma} \bar{n}_{i\bar{\sigma}} \bar{n}_{j\bar{\sigma}} n_{i'\sigma}$
  (b) $\sigma' = \bar{\sigma}$: $c_{i'\bar{\sigma}}^{\dagger} c_{i\bar{\sigma}} c_{i\sigma}^{\dagger} c_{j\sigma} n_{i'\sigma} \bar{n}_{j\bar{\sigma}}$.

In the other cases, the commutator becomes zero. Here, $[\hat{g}_{ij\sigma}, \hat{h}_{i'j'\sigma'}]$ can be obtained by considering the Hermitian conjugate.

For $\hat{H}_{\text{eff},3}^{(2)}$, we need to evaluate $[\hat{h}_{ij\sigma}^{\dagger}, \hat{h}_{i'j'\sigma'}]$, which can be expressed as follows:

(1) $i' = i$, $j' = j$
  (a) $\sigma' = \sigma$: $n_{i\bar{\sigma}} \bar{n}_{j\bar{\sigma}} (n_{i\sigma} - n_{j\sigma})$
  This term corresponds to the exchange couplings of the Z component in the spin Hamiltonian in Eq. (12) and the pseudospin Hamiltonian in Eq. (14).
  (b) $\sigma' = \bar{\sigma}$: $-c_{j\bar{\sigma}}^{\dagger} c_{i\bar{\sigma}} c_{i\sigma}^{\dagger} c_{j\sigma}$
  This term corresponds to the exchange coupling of the XY component of the spin Hamiltonian in Eq. (12).
(2) $i' = j$, $j' = i$
  (a) $\sigma' = \sigma$: 0
  (b) $\sigma' = \bar{\sigma}$: $c_{i\sigma}^{\dagger} c_{j\sigma} c_{i\bar{\sigma}}^{\dagger} c_{j\bar{\sigma}}$
  This term corresponds to the exchange coupling of the XY component of the pseudospin Hamiltonian in Eq. (14).
(3) $i' = i$, $j' \neq j$
  (a) $\sigma' = \sigma$: $-c_{j'\sigma}^{\dagger} c_{j\sigma} n_{i\bar{\sigma}} \bar{n}_{j\bar{\sigma}} \bar{n}_{j'\bar{\sigma}}$
  (b) $\sigma' = \bar{\sigma}$: $-c_{j'\bar{\sigma}}^{\dagger} c_{i\bar{\sigma}} c_{i\sigma}^{\dagger} c_{j\sigma} \bar{n}_{j'\sigma} n_{j\bar{\sigma}}$
(4) $i' \neq i$, $j' = j$
  (a) $\sigma' = \sigma$: $c_{i\sigma}^{\dagger} c_{i'\sigma} n_{i\bar{\sigma}} \bar{n}_{j\bar{\sigma}} n_{i'\bar{\sigma}}$
  (b) $\sigma' = \bar{\sigma}$: $-c_{j\bar{\sigma}}^{\dagger} c_{i'\bar{\sigma}} c_{i\sigma}^{\dagger} c_{j\sigma} n_{i'\sigma} n_{i\bar{\sigma}}$
(5) $i' = j$, $j' \neq i$
  (a) $\sigma' = \sigma$: 0
  (b) $\sigma' = \bar{\sigma}$: $c_{i\sigma}^{\dagger} c_{j\sigma} c_{j'\bar{\sigma}}^{\dagger} c_{j\bar{\sigma}} n_{i\bar{\sigma}} \bar{n}_{j'\sigma}$
(6) $i' \neq j$, $j' = i$
  (a) $\sigma' = \sigma$: 0
  (b) $\sigma' = \bar{\sigma}$: $c_{i\sigma}^{\dagger} c_{j\sigma} c_{i\bar{\sigma}}^{\dagger} c_{i'\bar{\sigma}} \bar{n}_{j\bar{\sigma}} n_{i'\sigma}$.

APPENDIX C: SCALING WITH U

Here, we discuss how the behavior of relevant physical quantities scales with U. In Fig. 17, we compare systems with
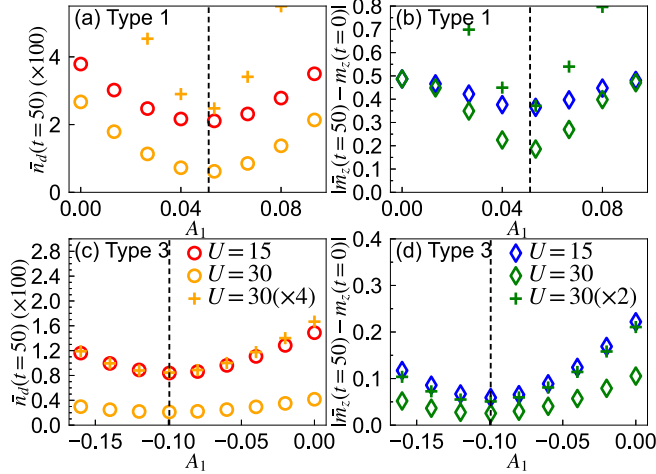
FIG. 17. Comparison of the doublon number and the staggered magnetization for $U = 15$ and 30. Both are averaged over a time interval $\frac{2\pi}{\Omega}$ around $t = 50$. The initial temperatures are $T = 0.02$ for $U = 15$ and $T = 0.01$ for $U = 30$. The parameters of the main electric field excitation are $\Omega = U/3$ and $A_0 = -1$. We set $l_0 = 3$, $n_1 = 3$, and $n_2 = 2$. The dashed lines indicate the optimal conditions for each protocol.

$U = 15$ and $30 (= 15 \times 2)$ and the type-1 and 3 protocols. For $U = 15$, the excitation conditions are the same as those in Figs. 8 and 9. For $U = 30$, the excitation frequencies are rescaled by a factor of 2, keeping the values of A_0, A_1, and δ_v. We note that, as in the case of $U = 15$, for $U = 30$, the heating is efficiently suppressed around the optimal conditions predicted by the Floquet Hamiltonian. In the type-1 protocol, the doublon number scales as $O(1/U^2)$ in the optimal condition. On the other hand, away from the optimal condition, the difference from the optimal case does not change with U. The reduction of the order parameter from the equilibrium value scales as $O(1/U)$ in the optimal condition. Away from the optimal condition, the difference from the optimal case is larger for $U = 30$. In the type-3 protocol, the doublon number scales as $O(1/U^2)$, while the reduction of the order parameter scales as $O(1/U)$.

We can understand the above behavior as follows. First, the equilibrium doublon number scales as $O(1/U^2)$, and the energy scale of the AFM order scales as $O(1/U)$. In the type-1 protocol with the optimal condition, the d-h creation term in the Floquet Hamiltonian scales as $O(1/U) (= O(1/\Omega))$ since the leading-order terms are canceled. Away from the optimal condition, the d-h creation term scales as $O(1)$. In the type-3 protocol, the d-h creation term scales as $O(1/U) (= O(1/\Omega))$. Note that, in this protocol, the optimal condition is chosen to minimize the d-h terms at the order of $1/\Omega$, but it never
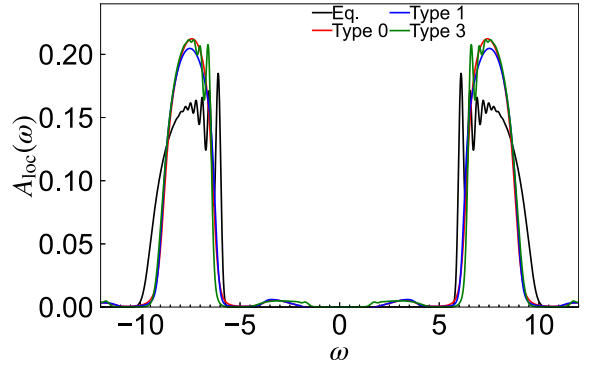

FIG. 18. Local single-particle spectral functions for $U = 15$ and $T = 0.02$ for the indicated systems. The parameters of the main electric field excitation are $\Omega = 5$ and $A_0 = -1$. For the auxiliary fields, we set $n_1 = 3$ and $n_2 = 2$ and use the optimal conditions determined from the Floquet Hamiltonian.

makes them zero. If we apply Fermi's golden rule for the d-h creation process, the d-h creation rate scales with the square of the coefficients of the d-h creation terms. The heating rate should also scale similarly. Moreover, the magnitude of the order reduction is determined by the ratio between the heating rate and the energy scale of the order. Thus, for example, in the type-3 protocol, the doublon number is expected to scale as $O(1/U^2)$. On the other hand, given that the energy scale of the AFM order is $O(1/U)$, the reduction of the magnetization should behave as $O(1/U)$. This consistently explains the numerical results. The behavior for the type-1 protocol can be explained analogously.

APPENDIX D: SPECTRAL FUNCTION UNDER EXCITATIONS

In Fig. 18, we compare the single-particle spectra $A_{\text{loc}}(\omega)$ evaluated for various cases. Here, the spectrum is defined as $A_{\text{loc}}^R(\omega) \equiv -\frac{1}{\pi} \text{Im} \int dt \exp[i\omega(t_0 - t)] G_{\text{loc}}^R(t_0, t)$, where $G_{\text{loc}}^R(t_0, t)$ is the retarded part of the local Green's function averaged over spins. We set $t_0 \simeq 60$. As we explained in Sec. III B, in equilibrium, there emerge peaks corresponding to the formation of spin polarons in the AFM phase. Under the electric field, the width of the Hubbard bands is reduced due to the dynamical localization effect [63]. The renormalized bandwidth is almost the same among the type-0, 1, and 3 protocols, which indicates that the effect of the auxiliary fields is minor here. In the case of the type-3 protocol, one can identify the spin polarons in the spectrum, which indicates that the AFM order is robust under this excitation. On the other hand, for the other two protocols, the AFM order is suppressed, and no spin polaron structures can be identified.

[1] A. Eckardt, Rev. Mod. Phys. **89**, 011004 (2017).

[2] T. Oka and S. Kitamura, Annu. Rev. Condens. Matter Phys. **10**, 387 (2019).

[3] A. de la Torre, D. M. Kennes, M. Claassen, S. Gerber, J. W. McIver, and M. A. Sentef, Rev. Mod. Phys. **93**, 041002 (2021).

[4] T. Oka and H. Aoki, Phys. Rev. B **79**, 081406(R) (2009).

[5] T. Kitagawa, T. Oka, A. Brataas, L. Fu, and E. Demler, Phys. Rev. B **84**, 235108 (2011).

[6] M. A. Sentef, M. Claassen, A. F. Kemper, B. Moritz, T. Oka, J. K. Freericks, and T. P. Devereaux, Nat. Commun. **6**, 7047 (2015).

[7] M. Schüler, U. De Giovannini, H. Hübener, A. Rubio, M. A. Sentef, T. P. Devereaux, and P. Werner, Phys. Rev. X **10**, 041013 (2020).

[8] K. Takasan, A. Daido, N. Kawakami, and Y. Yanase, Phys. Rev. B **95**, 134508 (2017).

[9] H. Dehghani, M. Hafezi, and P. Ghaemi, Phys. Rev. Res. **3**, 023039 (2021).

[10] S. Kitamura and H. Aoki, Commun. Phys. **5**, 174 (2022).

[11] D. H. Dunlap and V. M. Kenkre, Phys. Rev. B **34**, 3625 (1986).

[12] N. Tsuji, T. Oka, and H. Aoki, Phys. Rev. B **78**, 235124 (2008).

[13] M. Knap, M. Babadi, G. Refael, I. Martin, and E. Demler, Phys. Rev. B **94**, 214504 (2016).

[14] M. A. Sentef, Phys. Rev. B **95**, 205111 (2017).

[15] Y. Murakami, N. Tsuji, M. Eckstein, and P. Werner, Phys. Rev. B **96**, 045125 (2017).

[16] J. H. Mentink, K. Balzer, and M. Eckstein, Nat. Commun. **6**, 6708 (2015).

[17] M. Claassen, H.-C. Jiang, B. Moritz, and T. P. Devereaux, Nat. Commun. **8**, 1192 (2017).

[18] S. Kitamura, T. Oka, and H. Aoki, Phys. Rev. B **96**, 014406 (2017).

[19] N. Arakawa and K. Yonemitsu, Phys. Rev. B **103**, L100408 (2021).

[20] H. Lignier, C. Sias, D. Ciampini, Y. Singh, A. Zenesini, O. Morsch, and E. Arimondo, Phys. Rev. Lett. **99**, 220403 (2007).

[21] A. Eckardt, M. Holthaus, H. Lignier, A. Zenesini, D. Ciampini, O. Morsch, and E. Arimondo, Phys. Rev. A **79**, 013611 (2009).

[22] K. Sandholzer, Y. Murakami, F. Görg, J. Minguzzi, M. Messer, R. Desbuquois, M. Eckstein, P. Werner, and T. Esslinger, Phys. Rev. Lett. **123**, 193602 (2019).

[23] G. Jotzu, M. Messer, R. Desbuquois, M. Lebrat, T. Uehlinger, D. Greif, and T. Esslinger, Nature (London) **515**, 237 (2014).

[24] M. Aidelsburger, M. Lohse, C. Schweizer, M. Atala, J. U. T. Barreiro, S. Nascimbène, N. U. R. Cooper, I. Bloch, and N. Goldman, Nat. Phys. **11**, 162 (2015).

[25] F. Görg, M. Messer, K. Sandholzer, G. Jotzu, R. Desbuquois, and T. Esslinger, Nature (London) **553**, 481 (2018).

[26] J. W. McIver, B. Schulte, F.-U. Stein, T. Matsuyama, G. Jotzu, G. Meier, and A. Cavalleri, Nat. Phys. **16**, 38 (2020).

[27] S. A. Sato, J. W. McIver, M. Nuske, P. Tang, G. Jotzu, B. Schulte, H. Hübener, U. De Giovannini, L. Mathey, M. A. Sentef et al., Phys. Rev. B **99**, 214302 (2019).

[28] N. Yoshikawa, Y. Hirai, K. Ogawa, S. Okumura, K. Fujiwara, J. Ikeda, T. Koretsune, R. Arita, A. Mitra, A. Tsukazaki et al., arXiv:2209.11932.

[29] Y. Hirai, N. Yoshikawa, M. Kawaguchi, M. Hayashi, S. Okumura, T. Oka, and R. Shimano, arXiv:2301.06072 .

[30] J.-Y. Shan, M. Ye, H. Chu, S. Lee, J.-G. Park, L. Balents, and D. Hsieh, Nature (London) **600**, 235 (2021).

[31] K. Viebahn, J. Minguzzi, K. Sandholzer, A.-S. Walter, M. Sajnani, F. Görg, and T. Esslinger, Phys. Rev. X **11**, 011057 (2021).

[32] A. Castro, U. De Giovannini, S. A. Sato, H. Hübener, and A. Rubio, Phys. Rev. Res. **4**, 033213 (2022).

[33] O. Neufeld, N. Tancogne-Dejean, U. De Giovannini, H. Hübener, and A. Rubio, Phys. Rev. Lett. **127**, 126601 (2021).

[34] Y. Ikeda, S. Kitamura, and T. Morimoto, Prog. Theor. Exp. Phys. **2022**, 04A101 (2021).

[35] S. Sur, A. Udupa, and D. Sen, Phys. Rev. B **105**, 054423 (2022).

[36] Y. Wang, A.-S. Walter, G. Jotzu, and K. Viebahn, Phys. Rev. A **107**, 043309 (2023).

[37] A. Georges, G. Kotliar, W. Krauth, and M. J. Rozenberg, Rev. Mod. Phys. **68**, 13 (1996).

[38] H. Aoki, N. Tsuji, M. Eckstein, M. Kollar, T. Oka, and P. Werner, Rev. Mod. Phys. **86**, 779 (2014).

[39] A. Subedi, A. Cavalleri, and A. Georges, Phys. Rev. B **89**, 220301(R) (2014).

[40] R. Mankowsky, M. Först, and A. Cavalleri, Rep. Prog. Phys. **79**, 064503 (2016).

[41] D. Golež, J. Bonča, M. Mierzejewski, and L. Vidmar, Phys. Rev. B **89**, 165118 (2014).

[42] M. Eckstein and P. Werner, Sci. Rep. **6**, 21235 (2016).

[43] M. Bukov, M. Kolodrubetz, and A. Polkovnikov, Phys. Rev. Lett. **116**, 125301 (2016).

[44] M. Bukov, L. D'Alessio, and A. Polkovnikov, Adv. Phys. **64**, 139 (2015).

[45] A. Herrmann, Y. Murakami, M. Eckstein, and P. Werner, Europhys. Lett. **120**, 57001 (2017).

[46] S. Kitamura and H. Aoki, Phys. Rev. B **94**, 174503 (2016).

[47] M. Eckstein and P. Werner, Phys. Rev. B **82**, 115115 (2010).

[48] M. Schüler, D. Golež, Y. Murakami, N. Bittner, A. Herrmann, H. U. Strand, P. Werner, and M. Eckstein, Comput. Phys. Commun. **257**, 107484 (2020).

[49] P. Werner, H. U. R. Strand, S. Hoshino, and M. Eckstein, Phys. Rev. B **95**, 195405 (2017).

[50] P. Werner, H. U. R. Strand, S. Hoshino, Y. Murakami, and M. Eckstein, Phys. Rev. B **97**, 165119 (2018).

[51] J. Li, D. Golez, P. Werner, and M. Eckstein, Phys. Rev. B **102**, 165136 (2020).

[52] Y. Murakami, K. Uchida, A. Koga, K. Tanaka, and P. Werner, Phys. Rev. Lett. **129**, 157401 (2022).

[53] G. Martinez and P. Horsch, Phys. Rev. B **44**, 317 (1991).

[54] E. Dagotto, Rev. Mod. Phys. **66**, 763 (1994).

[55] G. Sangiovanni, A. Toschi, E. Koch, K. Held, M. Capone, C. Castellani, O. Gunnarsson, S.-K. Mo, J. W. Allen, H.-D. Kim et al., Phys. Rev. B **73**, 205121 (2006).

[56] S. A. Weidinger and M. Knap, Sci. Rep. **7**, 45382 (2017).

[57] J. H. Mentink and M. Eckstein, Phys. Rev. Lett. **113**, 057201 (2014).

[58] Y. Murakami, S. Takayoshi, T. Kaneko, A. M. Läuchli, and P. Werner, Phys. Rev. Lett. **130**, 106501 (2023).

[59] R. Arita, T. Miyake, T. Kotani, M. van Schilfgaarde, T. Oka, K. Kuroki, Y. Nozue, and H. Aoki, Phys. Rev. B **69**, 195106 (2004).

[60] K. Nakamura, T. Koretsune, and R. Arita, Phys. Rev. B **80**, 174420 (2009).

[61] Y. Murakami, S. Takayoshi, A. Koga, and P. Werner, Phys. Rev. B **103**, 035110 (2021).

[62] S. Imai, A. Ono, and S. Ishihara, Phys. Rev. Res. **4**, 043155 (2022).

[63] Y. Murakami and P. Werner, Phys. Rev. B **98**, 075102 (2018).